DOES FLUVIAL CHANNEL BELT CLUSTERING PREDICT NET SAND TO GROSS ROCK VOLUME?

ARCHITECTURAL METRICS AND POINT PATTERN ANALYSIS OF A DIGITAL OUTCROP MODEL

Alexander R. Koch[1] (alexrkoch@gmail.com), Cari L. Johnson[2] (cari.johnson@utah.edu), and Lisa Stright[3] (lisa.stright@colostate.edu)

[1] Chevron, Bakersfield, California 93311, U.S.A. (formerly University of Utah)

[2] Department of Geology and Geophysics, University of Utah, Salt Lake City, Utah 84112, U.S.A.

[3] Department of Geosciences, Colorado State University, Fort Collins, Colorado 80523, U.S.A.

ABSTRACT

Spatial point pattern analyses (PPAs) are used to quantify clustering, randomness, and uniformity of the distribution of channel belts in fluvial strata. Point patterns may reflect end-member fluvial architecture, e.g., uniform compensational stacking and avulsion-generated clustering, that may change laterally, especially at greater scales. To investigate spatial and temporal changes in fluvial systems, we performed PPA and architectural analyses on extensive outcrops of the Cretaceous John Henry Member of the Straight Cliffs Formation in southern Utah, USA. Digital outcrop models (DOMs) produced using unmanned aircraft system-based stereophotogrammetry form the basis of detailed interpretations of a ~250 m-thick fluvial succession over a total outcrop length of 4.5 km. The outcrops are oriented roughly perpendicular to fluvial transport direction. This transverse cross-sectional exposure of the fluvial system allows a study of the system's variation along depositional strike. We developed a workflow that examines spatial point patterns using the quadrat method, and architectural metrics such as net sand to gross rock volume (NTG), amalgamation index, and channel belt width and thickness within moving windows. Quadrat cell sizes that are ~50% of the average channel belt width-to-thickness ratio (16:1 aspect ratio) provide an optimized scale to investigate laterally elongate distributions of fluvial channel belt centroids. Large-scale quadrat point patterns were recognized using an array of 4 quadrat cells, each with 237x greater area than the median channel belt. Large-scale point patterns and NTG correlate negatively, which is a result of using centroid-based PPA on a dataset with disparately-sized channel belts. Small-scale quadrat point patterns were recognized using an array of 16 quadrat cells, each with 21x greater area than the median channel belt. Small-scale point patterns and NTG correlate positively, and match previously observed stratigraphic trends in the fluvial John Henry Member, suggesting that these are regional trends. There are deviations from these trends in architectural statistics over small distances (100s of meters) which are interpreted to reflect autogenic avulsion processes. Small-scale autogenic processes result in architecture that is difficult to correlate between 1D datasets, for example when characterizing a reservoir using well logs. We show that 1D NTG provides the most accurate prediction for surrounding 2D architecture.

INTRODUCTION

The architecture of fluvial deposits records complex interactions between allogenic and autogenic processes. Quantified parameters that are commonly used to help define stratigraphic architecture in fluvial deposits include net sand to gross rock volume (NTG; 'N' in Lake and

Jensen 1991), channel belt amalgamation (Allen 1979), and channel belt width and thickness (Gibling 2006), as well as paleomorphodynamic reconstructions based on grain size and estimates of bankfull depth (Paola and Mohrig 1996; Hajek and Heller 2012; Benhallam et al. 2016). Sandstone body density and interconnectedness (essentially NTG and amalgamation, respectively) were the key subjects of early modeling work by Leeder (1978), Allen (1978), and Bridge and Leeder (1979), known collectively as the LAB models (Paola 2000). These two architectural characteristics of fluvial strata strongly impact reservoir quality by determining the volume of connected porous rock capable of hosting hydrocarbons or water (Larue and Hovadik 2006). Models of fluvial architecture are frequently 2D or 3D while subsurface resource investigations often rely primarily on 1D borehole data. Detailed digital outcrop datasets allow us to connect 1D data to 2D outcrop architectural data and expand to 3D architectural prediction.

Sequence stratigraphic models link fluvial architecture with different stages of a relative sea level curve, notably predicting valley incision during lowstand regression which can later be filled by clustered channel belts (Posamentier and Vail 1988; Shanley and McCabe 1993; Wright and Marriott 1993). These models broadly infer allogenic controls of climate, tectonics, and eustasy based on fluvial architecture. Subsequent work building on the LAB models demonstrated the importance of autogenic processes such as avulsion in the development of fluvial architecture (Heller and Paola 1996; Hajek et al. 2010; Hajek and Straub 2017). Additionally, models of distributive fluvial systems (DFSs) (Weissmann et al. 2010), suggest predictable trends in NTG, amalgamation, and channel belt size, dependent on position relative to the DFS axis and its evolution over time (Owen et al. 2015).

Point pattern analysis (PPA) is a class of methods used to categorize spatial point patterns and classify points as randomly, clustered, or uniformly spaced (Cressie 1993). PPA has been applied to test for clustering in fluvial architecture and to compare outcrops to conceptual and physical models (Hajek et al. 2010; Hofmann et al. 2011; Flood and Hampson 2015; Chamberlin et al. 2016; Benhallam et al. 2016). Results from PPA quantify the spatial arrangement of points in 2D space (Cressie 1993). PPA is typically applied to fluvial deposits by treating each channel belt as a single centroid point and then analyzing their distribution over the study area (Hajek et al. 2010). Reducing complex channel belts to their centroid points is necessary using current PPA methods, but is an oversimplification and therefore potentially limits the usefulness of PPA (Hajek et al. 2010; Benhallam et al. 2016). For example, an asymmetric channel belt may have a centroid point that does not serve as an accurate center of mass for that sand body, and thus could not be used to describe NTG. However, the specific consequences of simplifying channel belts to centroid points are relatively unknown.

Clustering of channel belts has been attributed to allogenic controls, such as valley incision caused by base-level fall (e.g., Shanley and McCabe 1993) as well as autogenic controls, like avulsion (Hajek et al. 2010; Hajek et al. 2012; Huling and Holbrook 2016). Uniformity of channel belts and of channel belt clusters may reflect compensational stacking, whereby a river preferentially occupies the lowest topography on the floodplain, avoiding previous channel belts or channel belt clusters (Mohrig et al. 2000; Straub et al. 2009; Hofmann et al. 2011; Chamberlin et al. 2016). Point patterns, and to a large extent architectural metrics, have previously been used to highlight stratigraphic trends and their variation down-depositional-dip (Flood and Hampson 2015, Benhallam et al. 2016).

Leveraging a well-studied outcrop of the fluvial John Henry Member in southern Utah, this study seeks to: 1) quantify lateral and vertical trends in channel belt NTG, degree of amalgamation, width and thickness, and spatial point pattern using 4.5 km of depositional-strike-oriented outcrop to compare to previously studied outcrops along depositional-dip, 2) quantify the correlation between NTG and clustering, 3) describe specific characteristics of a fluvial dataset that could lead to more reliable results when using centroid-based PPA, and 4) test the limitations of 1D prediction by correlating 1D metrics to corresponding 2D architectural metrics. The results of this study can be used to guide 2D and 3D facies modeling of fluvial strata, which is highly useful in the exploration and development of hydrocarbons and water. This study adds to a growing body of literature which utilizes DOMs to supplement traditional outcrop data.

GEOLOGIC BACKGROUND

The Cretaceous John Henry Member of the Straight Cliffs Formation (southern Utah, USA) serves as an excellent laboratory to evaluate the spatial trends in fluvial channel belt architecture due to a long (~40 km) continuous depositional-strike-oriented outcrop exposure of fluvial deposits along the south-western margin of the Kaiparowits Plateau, known as the Cockscomb (Fig. 1). Numerous studies provide excellent sedimentologic and stratigraphic context for these strata and their down-depositional-dip paralic and marine equivalents (Peterson 1969a, 1969b; Shanley and McCabe 1991, 1993, 1995; Allen and Johnson 2010a, 2010b, 2011; Gallin et al. 2010; Szwarc et al. 2015; Benhallam et al. 2016; Johnson et al. 2016; Gooley et al. 2016; Mulhern and Johnson 2017).

The John Henry Member was deposited in a retroarc foreland basin from mid-Coniacian to early Campanian time. Accommodation was generated by the Sevier fold-thrust belt and dynamic topography (Liu and Nummedal 2004; Painter and Carrapa 2013), with sediment supplied from the Mogollon Highlands to the south and the Cordilleran magmatic arc to the southwest, in addition to the orogenic belt to the west (Szwarc et al. 2015; Primm et al. 2017).

Down-depositional-dip trends in fluvial architecture have been studied in detail by documenting stratigraphic trends in fluvial style and analyzing channel belt point patterns from Rock House Cove to Bull Canyon (~20 km distance; Fig. 1; Gooley et al. 2016; Benhallam et al. 2016). Gooley et al. (2016) divided the John Henry Member into 7 depositional units (DUs) based on facies associations and fluvial architecture, and observed 2 consistent stratigraphic trends. Trend 1 shows a decrease in grain size, channel-belt frequency, and width of channel belts up through stratigraphy from DU-1 to DU-3, with a shift in channel geometry from braided to meandering with tidal influence. Trend 2 shows an increase in grain size, channel-belt frequency, and width of channel belts up through stratigraphy from DU-4 to DU-6, with a shift in channel geometry from meandering to braided (Gooley et al. 2016). This previous work establishes excellent context for a detailed, statistical analysis of fluvial architecture in the John Henry Member, particularly looking for the first time at trends laterally in the fluvial system (~N-S) rather than down-depositional-dip.

DATASET AND METHODS

Data Collection, Model Generation and Interpretation

The dataset for this study consists of two digital outcrop models (DOMs) of the John Henry Member, CC1 and CC5 (Fig. 1), and three measured stratigraphic sections (Fig. 1, CCX. 1-3). Lithology, grain size, sedimentary structures, bedding geometry, paleocurrent indicators, and cross-bed thicknesses were recorded for each measured section (supplemental data in Koch 2018). The basal and upper contacts of the John Henry Member are well-defined, regional correlation surfaces in this area (Figs. 2, 3; Primm et al. 2017; Gooley et al. 2016; Peterson 1969b).

An unmanned aircraft system, the DJI Phantom 3 Professional quadcopter, was used to collect georeferenced photographs of each outcrop. CC1 is one continuous model created from 378 photographs (Fig. 2) and is approximately 1.4 km long and 275 meters in thickness. CC5 is composed of two overlapping models made from 288 and 343 photographs (Fig. 3) and is approximately 3.1 km long and 220 meters in thickness. Photos were collected by flying a grid pattern across each outcrop, maintaining on average 70% overlap between adjacent photos.

DOMs were generated with Agisoft Photoscan Professional (version 1.2.5) using Structure-from-Motion stereophotogrammetry, a method by which common points are identified in images taken from different locations, and 3D locations of those points are triangulated (Westoby et al. 2012). This process is repeated for every common pixel from each photo of the dataset to generate a 3D point cloud. A tiled model is generated from the 3D point cloud which incorporates pixels from the source photographs resulting in a photorealistic 3D surface. The DOMs were georeferenced using remotely selected control points collected with a differential GPS (Trimble GeoExplorer 6000) paired with a laser rangefinder (TRUPULSE 360°B). Rather than using traditional ground control targets, features on the outcrop were targeted with the laser-dGPS pair and their position was then photographed and annotated. Detailed descriptions of the entire DOM workflow can be found in Westoby et al. (2012). The average resolution of each DOM is 3.5 cm/pixel, such that most decimeter-scale sedimentary features are readily identifiable.

In the DOMs, 104 channel belts were interpreted in outcrop CC1, and 265 in outcrop CC5 (Fig. 6). Channel belts were interpreted in Agisoft Photoscan (version 1.2.5) using the polyline tool by outlining prominent sandstone bodies in the model. Channel belt bounding surfaces were interpreted using the hierarchical methods of Miall (1988), where lower order surfaces are truncated by higher order surfaces. Channel belts are bound by 5th order surfaces: a laterally persistent erosive surface on the base, and a contact with floodplain facies or the erosional base of an overlying channel belt on the top (Miall 1988). Amalgamated 5th order surfaces between two distinct channel belts can be confused with 4th order surfaces, which result from major shifts in channel or bar migration without the channel abandoning its position. Distinguishing 5th from 4th order surfaces in the DOMs posed a challenge, and in highly amalgamated areas it is likely that some channel belt interpretations represent multiple amalgamated channel belts (Fig. 4). Where present, lower order surfaces (e.g., 2nd and 3rd order) aided in distinguishing distinct packaging. Measured sections aided minimally in making surface distinctions due to their limited intersection with the much larger model areas, however they provided ground-truthing where possible.

The strata of outcrops CC1 and CC5 are dipping between 30-40° to the E-SE. In order to correct polyline interpretations for their structural orientation, they were exported from Agisoft as shapefiles, and imported into Schlumberger's Petrel (Version 2015). In Petrel, they were translated and rotated until the bedding orientation was perpendicular to the horizon. The rotated polylines were again exported as a shapefile and imported into ESRI ArcMap (Version 10.3) to be projected in 2D, resulting in a clean cross-section of the polyline interpretations. The polylines were then corrected for broad folding (maximum limb dip of 1.9°) along the outcrop in order to make them as consistently horizontal as possible. Polylines were cut at the peak of a fold, rotated until horizontal, and rejoined. To determine where bedding was truly horizontal we followed the methods of Calvo and Ramos (2015), identifying flat channel belt tops as datums for the section. After structural correction of folding and 2D projection, the DOMs still have distortion related to the topography of the outcrop, such that some amount of error can be expected in all calculations and analyses. Current software is not capable of manipulating DOMs to fully compensate for the complex interaction of strata and topography. Polylines were converted to closed polygons, and their centroid points were calculated in ArcGIS. The structurally corrected channel belt polygons, including their centroids, the 2D area of each polygon (Fig. 5A), contact polylines between amalgamated channel belts, and channel belt basal polylines (Fig. 5B) were all exported as shapefiles from ArcMap, and imported into MATLAB for analysis.

Definition of Architectural Metrics

Net Sand to Gross Rock Volume (NTG).—NTG is calculated by:

$$NTG(2D) = \frac{\sum_{i=1}^{n} A_i}{A_T} \quad (1.1)$$

where A_i is the transverse cross-sectional area of channel belt *i* out of *n* channel belts, and A_T is the total area over which the analysis is performed, which in this study is a moving window (Fig. 5A). This analysis is performed in 2-dimensional (eq. 1.1), or 1D (eq. 1.2):

$$NTG(1D) = \frac{\sum_{i=1}^{n} Th_i}{Th_T} \quad (1.2)$$

where Th_i is the thickness of sandstone bed in a 1D section divided by the total thickness of the moving window, Th_T. *NTG* is presented in this study as a dimensionless fraction between 0 and 1, where 0 is 0% sandstone and 1 is 100% sandstone. This is a simplification of the true outcrop lithology because there are minor tabular sandstone beds in the overbank deposits, and there are minor mudstone beds within the channel deposits. At this scale of investigation, the vast majority of each channel fill is composed of sandstone (see measured sections in Figs. 2, 3).

Channel Belt Amalgamation Index.—An index to quantify the degree of amalgamation of channel belts (after Funk et al. 2012; Peter et al. 2017):

$$AI(2D) = \frac{\sum_{j=1}^{m} \quad LAmalgamated_j}{\sum_{i=1}^{n} \quad LBase_i} \quad (1.3)$$

Where $LAmalgamated_j$ is length of contact between two channel belts and is a pairwise statistic performed over *m* pairs where *m* = *n* -1 contacts, and when summed, equals the total length of all amalgamation contacts (Fig. 5B). $LBase_i$ is the length of the channel belt bases *i* over *n* channel belts, and when summed, is the total length of all channel belt bases. *AI*, then, is the ratio of the length of amalgamated contacts over the total length over which amalgamation could occur, or the proportion to potential amalgamation. This analysis is performed in 2-dimensional (eq. 1.3), or 1D (eq. 1.4):

$$AI(1D) = \frac{m}{n} \quad (1.4)$$

Where *m* is the number of amalgamation contacts and *n* is the total number of channel belt bases encountered in the 1D section. *AI* is presented in this study as a dimensionless fraction between 0 and 1.

Channel Belt Width and Thickness.—Channel belt width is the maximum horizontal extent of the channel belt, and is measured by subtracting the minimum x-coordinate from the maximum x-coordinate of each channel belt polygon. Channel belt thickness is calculated as the maximum vertical distance between two points on the top and base of the polygon having equal x-coordinates (Fig. 5C). Paleocurrent indicators collected for this study (n = 251) primarily from trough cross-bed axes and dune accretion surfaces indicate an average paleocurrent direction of 109.2°, with a standard deviation of 2.1° (Fig. 1). The mean direction is nearly normal (89.2°) to the average strike of the outcrop faces (020°), indicating that apparent widths, used for the entirety of this study, are close to true channel belt widths.

Vertical and Lateral Trends in Architectural Metrics

A 600m x 25m "moving window" is stepped over the data, in 50m lateral and 5 m vertical increments to quantify spatial trends in architectural metrics (Fig. 6i). A 1D observation was also collected from a vertical line positioned at the center of each moving window. For each lateral moving window position, an R^2 value was calculated between the vertical trends of 1D and 2D architectural metrics, to quantify how well a 1D (e.g., borehole) dataset characterizes the architecture laterally for 300 m on either side. A separate moving window, 25 m thick and spanning the entire width of the outcrop, was used to analyze gross vertical stratigraphic trends, also moving vertically by 5 m increments (Fig. 6ii). For all metrics, channel belts were cropped to the moving window, except for channel belt width calculations. For channel belt thickness measurements, channel belts were cropped to the moving window laterally but not vertically.

Point Pattern Analysis of Channel Belt Distribution

Point pattern analysis characterizes the distribution of a set of points over a finite 2D area. Each method tests the hypothesis of complete spatial randomness (CSR; Cressie 1993) which asserts that a random set of points in a finite 2D area will have a Poisson distribution, i.e., each point location is independent of all other points, and has equal probability of being at any location in the study area. The centroid point of each channel belt polygon is used as the input point to understand the distribution of channel belts across each outcrop. We use the quadrat method in this study for its compatibility with a moving window analysis, which allows for comparison to results from architectural data.

We use the methods of Benhallam et al. (2016), who presented the first application of the quadrat method to the organization of fluvial channel belts. The quadrat method overlays the study area (i.e., moving window area) with a grid of equally-sized rectangular cells, and counts the number of points within each cell. The variance of points within each rectangle is then divided by the mean to produce the cluster index. When variance and mean are equal (clustering index = 1) points are distributed randomly, when variance is greater than the mean (clustering index > 1) points are clustered, and when variance is less than the mean (clustering index <1) points are distributed uniformly (Fig. 7). A robust way to compare results to those that could have been produced by a random process is to generate 99 Monte Carlo simulations where the number of simulated points and the simulated 2D area are both equal to that of the measured dataset. Using the same moving window and quadrat cell size, the quadrat analysis is performed for each Monte Carlo simulation. The range of cluster indices produced by 99 simulations is considered possible by random process, and is used to determine the statistical significance of a cluster index produced by the measured data. Cluster indices from the actual data are considered uniformly distributed if they are lower than the simulation envelope, random if they are within the simulation envelope, and clustered if they are greater than the simulation envelope. Point patterns of channel belts groups are anisotropic, loosely matching the elongate geometry of the channel belts themselves (Fig. 6). To introduce anisotropy to the quadrat method, the cells of the quadrat grid are manipulated to have the desired aspect ratio (Fig. 6iii, iv, v).

The quadrat method is performed within moving windows to analyze vertical and lateral trends. We used three different scales – small, medium, and large – of quadrat cells (Fig. 6iii, iv, and v respectively). Quadrat cells for all scales are arranged in two rows. Table 1 summarizes the various moving window and quadrat cell dimensions for each scale of analysis. Just as for the architectural analysis, the moving window begins at the base of the outcrop at the northern end. After each quadrat analysis, the window is stepped vertically by 5 m, until the top of the window reaches the top of the outcrop. The window is then returned to the base of the outcrop, and steps 50 m laterally to the south. Vertical and lateral movement of the window continues in this pattern until the window has traversed the entire outcrop. To assess the similarity or difference between NTG and clustering we use Pearson's R^2 correlation coefficient. For each quadrat cell scale described above – small, medium, and large – NTG was averaged over the entire quadrat cell grid (i.e., moving window). The vertical moving window results of quadrat cluster index and NTG at the first lateral moving window position are used to compute an R^2 value. This method is repeated for each lateral moving window position, generating a series of R^2 values which represent how well the two characteristics' vertical trends match with changing lateral position across the outcrop.

RESULTS

Architectural Trends

General Architectural Trends.—The John Henry Member has broadly similar architectural trends at outcrops CC1 and CC5, with stratigraphic and lateral variability both between and within outcrops (Figs. 6, 8). Previous work divided the John Henry Member at Rock House Cove (6.5 km south of CC5) and Bull Canyon (17 km E-SE of CC5) into 7 depositional units (DUs) on the basis of architectural and sedimentological characteristics (Gooley et al. 2016; Benhallam et al. 2016). Similar trends and units are present in the study area, but are simplified into three main units (dashed lines in Fig. 6) which correspond to the DUs of Gooley et al. (2016) as follows: lower = DUs 0-2, middle = DUs 3-4, and upper = DUs 5-6. In outcrops CC1 and CC5, the lower and upper units have greater average NTG and amalgamation index, with wider and thicker channel belts. In contrast, the middle unit tends to have lower average NTG and amalgamation index, with narrower channel belts, which is consistent with the previous interpretations of Gooley et al. (2016).

Each outcrop was divided into lateral segments to facilitate the detailed description of lateral variability. CC1 is referred to in terms of northern and southern segments, and CC5 is referred to as northern, central, and southern segments (vertical hashed lines, Fig. 8). Moving window analyses highlight and quantify outcrop trends of NTG, amalgamation index, and channel belt width and thickness (Fig. 8A-H) whereas gross vertical stratigraphic analyses (Fig. 8I-P) show laterally-averaged trends in architectural metrics.

Net-to-Gross (NTG).—Window-averaged NTG for CC1 ranges from 0.04 to 0.76. The CC1 gross vertical analysis (Fig. 8I) reveals two key trends; 1) an upward decrease from the lower unit into the middle unit, and 2) an upward increase from the middle unit to the upper unit. The CC1 moving window analysis (Fig. 8A) reveals minor lateral variation where the lower unit decreases in NTG from north to south, and the upper unit increases in NTG from north to south (Fig. 9).

Window-averaged NTG for CC5 ranges from 0.002 to 0.56, with less overall NTG than CC1. The CC5 gross vertical analysis (Fig. 8J) reveals three key NTG trends; 1) a decrease from the lower unit to the middle unit, 2) an intermediate peak within the middle unit, and 3) an upward increase to the upper unit (Fig. 9). The CC5 moving window analysis (Fig. 8B) reveals high lateral variability primarily in the middle and upper units. The middle unit has isolated packages of high NTG in the central and southern segments. The upper unit has increasing NTG from north to south. Thus, although overall NTG trends are similar across the study area, CC1 has less lateral variability than CC5.

Amalgamation Index.—For both outcrops, amalgamation index closely mimics the trends of NTG. Window-averaged amalgamation index for CC1 ranges from 0 to 0.65. The CC1 gross vertical analysis (Fig. 8K) reveals two key amalgamation index trends; 1) an upward decrease from the lower unit into the middle unit, and 2) and upward increase from the middle unit to the upper unit. The CC1 moving window analysis (Fig. 8C) reveals high lateral variability where amalgamation index in the lower unit decreases from north to south, and in the upper unit increases from north to south (Fig. 9).

Window-averaged amalgamation index for CC5 ranges from 0 to 0.65. The CC5 gross vertical analysis (Fig. 8L) for amalgamation index is more sporadic and irregular than CC5 NTG, however it loosely holds the same three trends; 1) a decrease from the lower unit to the middle unit, 2) an intermediate peak within the middle unit, and 3) an upward increase to the upper unit (Fig. 9). The CC5 moving window analysis (Fig. 8D) reveals high lateral variability in all units, where amalgamation index increases from north to south. The lower and middle units contain isolated packages of high amalgamation index, where the upper unit contains more laterally continuous amalgamated packages.

Channel Belt Thickness.— Channel belt thicknesses for CC1 range from 1.2 m to 14.2 m, with a mean of 5.2 m (Fig. 10). The CC1 gross vertical analysis (Fig. 8M) reveals two key channel belt thickness trends; 1) an upward decrease from the lower unit into the middle unit, and 2) an upward increase from the middle unit to the upper unit. The CC1 moving window analysis (Fig. 8E) reveals moderate lateral variation of channel belt thickness that mimics the NTG and amalgamation index trends in the lower unit, where channel belt thickness decreases from north to south. Channel belt thickness in the upper unit also decreases from north to south (Fig. 9).

Channel belt thicknesses for CC5 range from 0.3 m to 13.1 m, with a mean of 4.2 m (Fig. 10). The CC5 gross vertical analysis (Fig. 8N) reveals three key channel belt thickness trends; 1) a minor decrease from the lower unit to the middle unit, 2) a more significant upward increase to the middle unit-upper unit contact, and 3) a decrease within the upper unit. This third trend is unique to this analysis, and is caused by high lateral variability, as revealed in the CC5 moving window analysis in all stratigraphic units (Fig. 8F). The lower unit channel belt thicknesses decrease moderately from north to south. The middle unit channel belt thicknesses increase from the northern to the central segment, then decrease from the central to the southern segment. The upper unit has an inverse trend, where its channel belt thicknesses decrease from the northern to the central segments, then increase from the central to the southern segments (Fig. 9).

Channel Belt Width.— Apparent channel belt widths for CC1 range from 15.6 m to 1340 m, with a mean of 191.5 m (Fig. 10). The CC1 gross vertical analysis (Fig. 8O) reveals two key channel belt width trends; 1) an upward decrease from the lower unit into the middle unit, and 2) and upward increase from the middle unit to the upper unit. The CC1 moving window analysis (Fig. 8G) reveals moderate lateral variation that trends opposite the lateral variation of NTG and amalgamation index, where the lower unit increases in average channel belt width from north to south, and the upper unit decreases in average channel belt width from north to south (Fig. 9).

Channel belt widths for CC5 range from 8.6 m to 2450.1 m, with a mean of 127.3 m (Fig. 10). The CC5 gross vertical analysis (Fig. 8P) reveals two key channel belt width trends; 1) a moderate decrease from the lower unit to the middle unit, and 2) a more significant upward increase to the upper unit. The CC5 moving window analysis (Fig. 8H) reveals moderate lateral variability primarily in the middle and upper units. The middle unit channel belt widths increase from the northern to the central segments, then decrease from the central to the southern segments. The upper unit has an inverse trend, where it decreases from the northern to the central segments, then increases from the central to the southern segments (Fig. 9).

Point Pattern Analysis of Channel Belt Centroids

We analyzed small-, medium-, and large-scale point patterns of channel belt centroids for outcrop CC5, and only medium-scale point patterns for CC1. Beginning with CC5, at small point pattern scales with 16:1 aspect ratio quadrat cells (Fig. 6iii), this outcrop is dominated by clustering in the lower and upper units, and by uniformity and randomness in the middle unit (Fig. 11A). Small scale point patterns of CC5 have low lateral variability. The lower unit has the most clustering in the southern segment, and the upper unit has the most clustering in the central unit. At medium point pattern scales (Fig. 6iv), outcrop CC5 has high lateral variability with two main categories of clustering; a) major clustering in the lower and middle units in the central and southern segments, and b) very sparse clustering throughout the upper unit (Fig. 11C). Elsewhere, the medium scale CC5 analysis is dominated by randomness with sparse uniformity. At large point pattern scales with 16:1 aspect ratio quadrat cells (Fig. 6v), outcrop CC5 is dominated by clustering in the lower unit and lower half of the middle unit, with very sparse uniformity in the middle unit of the central and southern segments (Fig. 11B). Laterally, large-scale clustering has low variability, with a slight increase in abundance from north to south.

At medium point pattern scales with a low aspect ratio of 2.4:1, outcrop CC1 has high lateral variability with two regions of high clustering; a) the middle to upper unit in the northern segment, and b) the lower to middle unit in the southern segment (Fig. 11D). The CC1 quadrat analysis also shows two regions of uniformity; a) the lower unit in the northern segment, and b) the middle unit in the southern segment.

Correlation of Point Pattern Results to NTG

Correlations between quadrat point pattern results and NTG are summarized in Figure 11E-H. In outcrop CC5, small scale point patterns have a weak-to-moderate positive correlation to NTG, with a mean R^2 value of 0.32, and a standard deviation of 0.14 (Fig. 11E). In contrast, large-scale point patterns have a moderate-to-strong negative correlation to NTG, with a mean R^2 value of -0.61, and a standard deviation of 0.10 (Fig. 11F). The medium scale analyses for both CC5 and CC1 have correlations with high lateral variability. Medium scale point patterns of outcrop CC5 have a strong positive correlation to NTG in the north, and a moderate negative correlation in the central and the southern portions of the outcrop (Fig. 11G). Medium scale point patterns of outcrop CC1 have a strong negative correlation to NTG in the north, non-correlation in the center of the outcrop, and a strong positive correlation in the south (Fig. 11H)

Correlation of 1D and 2D Channel Belt NTG, Amalgamation Index, and Thickness.

Correlations between 1D and 2D channel belt NTG, amalgamation index, and thickness are summarized in Figure 12. Channel belt width and point pattern cannot be measured in a vertical 1D section so they were omitted for this analysis. For both outcrops, NTG has the strongest correlation between 1D and 2D, with a mean R^2 value of 0.93 for CC1, and 0.78 for CC5. NTG also has the lowest standard deviation in R^2 values of each lateral window, at 0.02 for CC1, and 0.09 for CC5. The metric with the second strongest correlation is different for each outcrop. For CC1, amalgamation index is second best ($R^2 = 0.68$), and for CC5 thickness is second best ($R^2 = 0.54$). The least correlative features for each outcrop are thickness for CC1 ($R^2 = 0.57$), and amalgamation index for CC5 ($R^2 = 0.41$).

DISCUSSION

Methodology of Point Pattern Analysis

Point pattern analysis permits statistical characterization of feature clustering, and thus is a potentially powerful tool for quantifying aspects of fluvial architecture (Hajek and Wolinsky 2012). PPA methods have been used to investigate avulsion behavior and characterize stratigraphic patterns (Hajek et al. 2010; Flood and Hampson 2015; Chamberlin et al. 2016; Benhallam et al. 2016). PPA methodology applied to fluvial deposits is still relatively new, and only a few methods have been tested on a limited number of outcrops such as the Cretaceous Ferris, Blackhawk, and Williams Fork Formations, as well as other outcrops of the John Henry Member to the south and southeast of the Cockscomb (Hajek et al. 2010; Flood and Hampson 2015; Chamberlin et al. 2016; Benhallam et al. 2016). Outcrops CC1 and CC5 are laterally extensive, permitting the analysis of point patterns and fluvial architecture at a variety of scales. The results reveal dataset-size guidelines for any PPA method, provided that the data set is similar in scale and channel belt density to CC1 and CC5. In total, CC1 and CC5 cover an area 4.5 km wide by 250 m tall, and have on average 4 channel belts per 100 m^2. Channel belt centroids are spaced 12 m apart laterally on average.

To date, point pattern techniques used in fluvial stratigraphy have mostly been isotropic, searching for point patterns occupying an equant space (Hajek et al. 2010; Chamberlin et al. 2016). In contrast, Flood and Hampson (2015) vertically exaggerated their channel belt point set to incorporate anisotropy into the analysis, and Benhallam et al. (2016) used quadrat cells with width-to-thickness ratios higher than 1:1. For the approach of Flood and Hampson, vertical exaggeration by a factor of x results in an analysis capable of identifying point patterns with x:1 width-to-thickness ratio, which better matches the elongate channel belt geometry of most fluvial deposits. Flood and Hampson (2015) used the ratio of mean channel belt width to mean channel belt thickness as the vertical exaggeration factor. By qualitatively identifying clusters in the present dataset, we determined that approximately half the ratio of mean channel belt width to mean channel belt thickness (16:1 for the Cockscomb) should produce the most geologically realistic results, i.e., this ratio highlights geologically relevant clusters rather than artifacts or outlier signals. This aspect ratio was applied in the quadrat method following Benhallam et al. (2016) by using cells of the desired aspect ratio. Further work is needed, particularly statistical analysis using data from many different field examples, to empirically determine the most common aspect ratios of channel belt clusters. Until such a dataset is compiled, workers applying anisotropic point pattern techniques should perform sensitivity analysis on a range of aspect ratios, as well as search for qualitative evidence of clusters within their dataset.

Scale flexibility is limited in the quadrat method, because the moving window must be evenly divisible by the size of the quadrat cells in both dimensions, so tailoring the experiment to the exact point pattern scale and aspect ratio can be inconvenient. However, the quadrat method's requirement of fitting equally within the window boundaries means it requires no edge correction.There is an inherent problem with edge effects in any PPA method, because all outcrops have finite dimensions. For our purposes and for the present dataset, we argue that the quadrat method is most appropriate. Our results indicate that a minimum total data frame width (i.e., a moving window in this study) should be at least 500 m for the average lateral centroid spacing of 12 m in the present dataset. This is the size necessary to have observed the small-scale clusters of outcrop CC5. Edge effects will decrease as the data frame increases width beyond 500 m. In order to observe large-scale clusters accurately, the results indicate that a dataset with total width >3 km is optimal.

Correlation of Point Patterns and Net-to-Gross

How do fluvial architectural properties statistically relate to point patterns? Clustering is the presence of channel belts in close proximity to one another compared to surrounding channel deposits. Therefore, we focused on NTG to answer this question. Clustered channel deposits have been previously identified as having high relative NTG (Hofmann et al. 2011), increased channel belt width and thickness, and elevated amalgamation (Benhallam et al. 2016).

At small point pattern scales, clustering and NTG have a weak positive correlation (Fig. 11E). The stratigraphic trends of small scale clustering and NTG found in outcrop CC5 match those found by Benhallam et al. (2016) at nearby outcrops of Rock House Cove and Bull Canyon (Fig. 1). There is an upward decrease in clustering and NTG from the base to the middle of the section, followed by an upward increase from the middle to the top of the section (Fig. 12 of Benhallam et al. 2016). However, at medium and large scales, clustering and NTG within outcrops CC5 and CC1 are mostly negatively correlated, or highly variable resulting in non-correlation on average (Fig. 11F-H). To explain these anti-correlative results, we consider two possible interpretations: 1) the methodology is fundamentally flawed, because analyzing point patterns using centroids cannot accurately describe the spatial arrangement of fluvial channel belts of disparate geometry, and/or 2) the methods are reasonably accurate and this signal is true, indicating that large-scale clusters tend to be composed of smaller channel belts resulting in a lower total NTG than their larger, uniform and random counterparts.

Although these two interpretations may be compatible to some degree, we favor the notion that the methodology for identifying large-scale point patterns has high error. Primarily, this inaccuracy is due to the simplification of each channel belt to a single point for PPA, which previous studies suggested was likely problematic (e.g., Hajek et al. 2010; Benhallam et al. 2016). However, in previous work there has been no quantification of the geometry (area, width, thickness) of channel belts in a way that can be statistically compared to PPA results. The apparent anti-correlation of large-scale clustering to NTG in outcrop CC5 provides quantitative evidence that centroid-based PPA cannot accurately describe large-scale fluvial architecture for the present dataset. The ability of centroid-based PPA to characterize architecture is influenced by the variety of channel belt widths within the dataset, and the resolution of internal architecture of large channel belts. Our interpretation of this PPA methodological pitfall could be tested in future work by repeating the correlation exercise but using vertical rather than lateral moving windows. Anti-correlation in a vertical moving window correlation would corroborate our current hypothesis, whereas correlation would raise new questions.

Both CC5 and CC1 have significant stratigraphic variation in the width of channel belts (Fig. 8G and H). The lower and middle units of CC5 result in large-scale clusters that are composed of more numerous and narrower channel belts, resulting in lower total NTG (Figs. 8, 11). In contrast, the highest NTG values of outcrop CC5 are associated with a series of very wide (>1 km: 1/3 total outcrop width) channel belts in the upper unit of the southern segment (Figs. 8B and H). In outcrops with disparate channel belt widths, the narrower belts produce higher point density, whereas the wider, laterally amalgamated channel belts have fewer centroids, resulting in lower point density. When the two distinct styles of channel belts are juxtaposed in the quadrat method, the area with higher point density has a greater chance of having variance of points-per-cell much greater than the mean, resulting in a high clustering index. This variety of channel belt widths occurring together is common in the John Henry Member, and many other fluvial successions worldwide (e.g., Robinson and McCabe 1997; Bridge et al. 2000; Rittersbacher et al. 2014; Flood and Hampson 2015). We predict that PPA and NTG proxy one another more accurately when the dataset has a low range of channel belt widths. Small-scale analysis shows a stronger positive correlation because a smaller moving window, especially in the vertical dimension, incorporates a lower variety of channel belt geometries.

Wide channel belts were likely deposited via post-avulsion lateral migration of a river, rather than purely aggradational filling of a very wide river (Gibling 2006). It is also likely that many of these wide belts were formed by multiple generations of avulsion, reoccupation, and lateral river migration (Leeder 1978; Bridge 1993; Larue and Hovadik 2006). From certain portions of the CC1 and CC5 models with exceptionally high resolution, and from outcrop analysis, detailed internal architecture exists that is not observable in the majority of each DOM (Fig. 4). Bounding surfaces that indicate avulsion (5th-order) are often difficult to differentiate from 4th-order surfaces which indicate a major change in the migration of a river or barform, rather than an avulsion (surfaces labeled “4/5?” in Fig. 4; Miall 1988).

Further evidence for avulsion-generated sand bodies includes irregular 'sawtooth' channel margins, and correlation of individual channel stories with floodplain horizons laterally (Chamberlin and Hajek 2015). For very wide channel belts, both of these observations are limited. Many of the channel margin contacts are sand-on-sand, so irregularity in the margin geometry is difficult to detect. In these and many other fluvial outcrops, floodplain deposits are poorly exposed, making their correlation to channel belt stories difficult. Without internal architectural geometry, i.e., a clear 5th order surface indicating incision and establishment of a new channel (Miall 1988), the location of the avulsion that initiated a wide channel belt and the location of any avulsions that came later are both unclear. Because of this uncertainty, the centroid point is a poor approximation of avulsion location for channel belts that are much wider than estimated paleo-river width. The use of PPA to understand avulsion dynamics becomes more reliable with better understanding of internal architecture of wider and more complex channel belts. If internal architecture is not readily interpretable, PPA is more effective when channel belt width is closer to estimated paleo-river width.

Correlation of Architectural Metrics from 1D to 2D

Subsurface resource investigations rely heavily on 1D borehole data collected at multiple locations across an area of interest. Correlation between 1D datasets can inform a 2D or 3D interpretation of the subsurface architecture. The present outcrop dataset provides an excellent opportunity to collect 1D measurements of NTG, channel belt amalgamation index, and channel belt thickness in a hypothetical borehole. For each of these architectural metrics we determined how similar the 1D dataset is to the 2D moving window extending 300 m away from the hypothetical borehole in either direction. The results show that consistently for both outcrops NTG has the highest predictivity from 1D to 2D compared to the other two metrics (Fig. 12). Channel belt amalgamation index and thickness did not have a consistent pattern, varying in their predictivity from 1D to 2D within and between outcrops CC1 and CC5. For example, 1D measurements of amalgamation index in outcrop CC5 are negatively correlated to their surrounding 2D area in the north, but in the south they are positively correlated. Over the scale of 100s to 1000s of meters along strike, channel belt amalgamation index and thickness are unreliable 1D to 2D predictors, while NTG is very reliable.

Controls on Sedimentation

Small-scale clustering, NTG, amalgamation index, and channel belt width and thickness along the Cockscomb broadly follow two key stratigraphic trends; Trend 1 is a decrease in all metrics from the lower unit to the middle unit, and Trend 2 is an increase in all metrics from the middle unit to the upper unit. These trends are regionally persistent, spanning at least 15 km south to Rock House Cove and 20 km southeast to Bull Canyon (Figs. 1, 9; Gooley et al. 2016; Benhallam et al. 2016). The 600 m-wide moving window analysis reveals significant lateral variation from these key trends, on the order of 100s to 1000 m. In outcrop CC5 there are multiple isolated packages of higher NTG, amalgamation index, and channel belt width and thickness in the middle unit, disrupting the broad up-section decreasing-to-increasing trends (Figs. 8, 9). These trends are the result of clustered large channel belts, which stand out in the relatively low-NTG middle unit (Fig. 6). We interpret these clusters to be formed by autogenic processes because they contradict trends observed regionally, and they themselves do not form a regionally persistent pattern (Hajek and Straub 2017). A possible autogenic mechanism for the generation of these clusters is via preferred re-occupation of an abandoned channel by an avulsing river (Mohrig et al. 2000; Jerolmack and Paola 2007; McHargue et al. 2011).

Autogenic processes are likely always important signals in a fluvial system (Budd et al. 2016; Paola 2016), but broad changes in fluvial style, such as those associated with Trends 1 and 2, may represent changing allogenic forces which influence autogenic processes. Gooley et al. (2016) suggest that Trend 1 is caused by a primarily tectonically driven relative base-level fall, followed by a time of high accommodation coeval to transgressive shoreline deposits down-depositional-dip. Trend 2 records the autogenic progradation of a distributive fluvial system influenced by tectonic subsidence and increased sediment supply (Gooley et al. 2016). The results of this study corroborate the conclusions of Gooley et al. (2016) but do not allow for further refinement of controls on sedimentation. An important caveat to the interpretation of Trend 2 is that the general scale of DFSs is much greater than the scale of observation for this study. Modern DFSs range in width from 10s to 100s of km (Weissmann et al., 2010; Hartley et al., 2010). The Salt Wash DFS is estimated to be ~450 km wide based on maps from Owen et al. (2015). Thus, the scale of observation for this study is significantly smaller than the full scale of the DFS, such that only a portion of the DFS is observed (Primm et al. 2017).

CONCLUSIONS

This study adds to a growing body of literature that utilizes statistical methods to understand the character and organization of fluvial channel deposits. We investigated point patterns and architectural metrics in the John Henry Member, and the correlation between the two at different scales. The studied outcrops are ideal for this type of analysis due to their scale and orientation roughly perpendicular to paleoflow. The outcrops used in this work comprise a total of 4.5 km of along-strike exposure, with an average stratigraphic thickness of 250 m, containing a total of 369 interpreted channel belts. Point patterns and architectural metrics broadly follow two key stratigraphic trends: Trend 1, an upward decrease from the base to the middle of the section, and Trend 2, an upward increase from the middle to the top of the section. There is divergence from these trends along depositional strike as architecture varies at small scales (100s of meters) and large scales (kilometers). Small scale, and possibly larger scale, variation is likely caused by autogenic dynamics of the fluvial system, such as avulsion.

Autogenic processes are thought to be influenced by allogenic forces, such as climate, tectonics, eustasy, and dynamic mantle topography, resulting in the broad consistency of Trends 1 and 2.

Subsurface resource investigations rely heavily on interpolation between 1D borehole data points in order to interpret 2D and 3D architecture. Results from the 1D-2D correlation show that 1D NTG is more useful than 1D amalgamation index or channel belt thickness for predicting the surrounding 2D architecture. While amalgamation index and channel belt thickness have a high positive 1D-2D correlation across some portions of the outcrop, NTG has a consistently high positive correlation at all lateral positions of both outcrops.

Channel belt clustering predicts net-to-gross when channel belt architecture is uniform laterally and vertically, a situation that is unlikely to be encountered at all scales of any fluvial system. At small point pattern scales (quadrat cells 21x greater area than the median channel belt), channel belt clustering and NTG are positively correlated and both broadly follow two key trends: Trend 1, an upward decrease from the base to the middle of the section, and Trend 2, an upward increase from the middle to the top of the section. These trends were also described by previous workers as far as 15 km to the south, and 20 km to the southeast, along a depositional dip profile (Gooley et al. 2016; Benhallam et al. 2016). In contrast, at medium and large point pattern scales (quadrat cells respectively 35x and 237x greater area than the median channel belt), clustering has a mostly negative correlation to NTG. This anti-correlation is the result of the simplification of channel belts to centroid points in the PPA analysis for an outcrop with a large range in channel belt sizes. In a dataset with high channel belt width variety, belts of disparate width are each represented equally by a single centroid. When they are juxtaposed in the same analysis, smaller, more abundant belts are more likely to result in clustering, which is then negatively correlated to NTG. A centroid approximation for PPA analysis is more effective when an outcrop is composed of uniformly-sized channel belts. For this same reason centroid approximation introduces uncertainty to using PPA to interpret paleoavulsion. Using centroids in avulsion analysis is more effective the closer channel belt width is to estimated paleoriver width, and when there is high confidence in the internal architecture of highly amalgamated channel belts.

ACKNOWLEDGEMENTS

This project was completed as part of the Rocks to Models consortium, funded by ConocoPhillips, Hess, and Shell. We thank the Bureau of Land Management and Grand Staircase–Escalante National Monument (GSENM) for allowing us to do field work on federal land. Field and lab support was generously provided by Shawn Moore, Jen Morris, Ellen Reat, Julia Mulhern, Aubry DeReuil, Gabby St. Pierre, Jon Primm, Casey Meirowitz, Cory Johnson, David Wheatley, Casey Duncan, Jeff Gay, and Spencer Hollingworth. We gratefully acknowledge the thoughtful reviews from Alessandro Ielpi and Jason Muhlbauer, which helped to improve the manuscript.

REFERENCES

Allen, J.R.L., 1979, Studies in fluviatile sedimentation: An elementary geometrical model for the connectedness of avulsion-related channel sand bodies: Sedimentary Geology, v. 24, p. 253–267.

Allen, J.R.L., 1978, Studies in fluviatile sedimentation: an exploratory quantitative model for the architecture of avulsion-controlled alluvial suites: Sedimentary Geology, v. 21, p. 129–147.

Allen, J.L., and Johnson, C.L., 2011, Architecture and formation of transgressive-regressive cycles in marginal marine strata of the John Henry Member, Straight Cliffs Formation, Upper Cretaceous of Southern Utah, USA: Sedimentology, v. 58, p. 1486–1513.

Allen, J.L., and Johnson, C.L., 2010a, Facies control on sandstone composition (and influence of statistical methods on interpretations) in the John Henry Member, Straight Cliffs Formation, Southern Utah, USA: Sedimentary Geology, v. 230, p. 60–76.

Allen, J.L., and Johnson, C.L., 2010b, Sedimentary facies, paleoenvironments, and relative sea level changes in the John Henry Member, Cretaceous Straight Cliffs Formation, Southern Utah, USA: Geology of South-Central Utah, v. 39, p. 225–247.

Benhallam, W., Turner, A., Stright, L., and Johnson, C.L., 2016, Spatial analysis of channel-belt stacking patterns: Metrics to discriminate between local and regional controls on deposition in the fluvial John Henry Member of the Straight Cliffs Formation, Southern Utah, U.S.A.: Journal of Sedimentary Research, v. 86, p. 1310–1327.

Bridge, J.S., 1993, The interaction between channel geometry, water flow, sediment transport and deposition in braided rivers: Geological Society, London, Special Publications, v. 75, p. 13–71.

Bridge, J.S., Jalfin, G. A, and Georgieff, S.M., 2000, Geometry, lithofacies, and spatial distribution of Cretaceous fluvial sandstone bodies, San Jorge Basin, Argentina: Outcrop analog for the hydrocarbon-bearing Chubut Group: Journal of Sedimentary Research, v. 70, p. 341–359.

Bridge, J.S., and Leeder, M.R., 1979, A simulation model of alluvial stratigraphy: Sedimentology, v. 26, p. 617–644.

Budd, D.A., Hajek, E.A., and Purkis, S.J., 2016, Autogenic dynamics and self-organization in sedimentary systems: SEPM (Society for Sedimentary Geology) Special Publication, no. 106.

Calvo, R., and Ramos, E., 2015, Unlocking the correlation in fluvial outcrops by using a DOM-derived virtual datum: Method description and field tests in the Huesca fluvial fan, Ebro Basin (Spain): Geosphere, v. 11, p. 1507–1529.

Chamberlin, E.P., and Hajek, E. A, 2015, Interpreting paleo-avulsion dynamics from multistory sand bodies: Journal of Sedimentary Research , v. 85, p. 82–94.

Chamberlin, E.P., Hajek, E.A., and Trampush, S.M., 2016, Measuring scales of autogenic organization in fluvial stratigraphy: An example from the Cretaceous Lower Williams Fork Formation, Colorado: Autogenic Dynamics in Sedimentary Systems: SEPM (Society for Sedimentary Geology) Special Publication, no. 106.

Cressie, N.A.C., 1993, Statistics for spatial data: New York, Wiley, 588 p.

Flood, Y.S., and Hampson, G.J., 2015, Quantitative analysis of the dimensions and distribution of channelized fluvial sandbodies within a large outcrop dataset: Upper Cretaceous Blackhawk formation, Wasatch Plateau, central Utah, U.S.A.: Journal of Sedimentary Research, v. 85, p. 315–336.

Funk, J. E., Slatt, R. M., and Pyles, D. R., 2012, Quantification of static connectivity between deep-water channels and stratigraphically adjacent architectural elements using outcrop analogs. AAPG Bulletin, v. 96, no. 2, p. 277–300.

Gallin, W.N., Johnson, C.L., and Allen, J.L., 2010, Fluvial and marginal marine architecture of the John Henry Member, Straight Cliffs Formation, Kelly Grade of the Kaiparowits Plateau, South-Central Utah: Geology of South-Central Utah, p. 248–275.

Gibling, M.R., 2006, Width and thickness of fluvial channel bodies and valley fills in the geological record: A literature compilation and classification: Journal of Sedimentary Research, v. 76, p. 731–770.

Gooley, J.T., Johnson, C.L., and Pettinga, L., 2016, Spatial and temporal variation of fluvial architecture in a prograding clastic wedge of the late Cretaceous Wester Interior Basin (Kaiparowits Plateau), U.S.A: Journal of Sedimentary Research, v. 86, p. 125–147.

Hajek, E.A., and Heller, P.L., 2012, Flow-depth scaling in alluvial architecture and nonmarine sequence stratigraphy: Example from the Castlegate Sandstone, Central Utah, U.S.A: Journal of Sedimentary Research, v. 82, p. 121–130.

Hajek, E.A., Heller, P.L., and Schur, E.L., 2012, Field test of autogenic control on alluvial stratigraphy (Ferris Formation, Upper Cretaceous-Paleogene, Wyoming): Bulletin of the Geological Society of America, v. 124, p. 1898–1912.

Hajek, E.A., Heller, P.L., and Sheets, B.A., 2010, Significance of channel-belt clustering in alluvial basins: Geology, v. 38, p. 535–538.

Hajek, E.A., and Straub, K.M., 2017, Autogenic sedimentation in clastic stratigraphy: Annu. Rev. Earth Planet. Sci, v. 45, p. 681–709.

Hajek, E.A., and Wolinsky, M.A., 2012, Simplified process modeling of river avulsion and alluvial architecture: Connecting models and field data: Sedimentary Geology, v. 257, p. 1-30.

Hartley, A.J., Weissmann, G.S., Nichols, G.J., and Warwick, G.L., 2010, Large distributive fluvial systems: Characteristics, distribution, and controls on development: Journal of Sedimentary Research, v. 80, p. 167-183.

Heller, P.L., and Paola, C., 1996, Downstream changes in alluvial architecture: An exploration of controls on channel-stacking patterns: Journal of Sedimentary Research, v. 66, p. 197–306.

Hofmann, M.H., Wroblewski, A., and Boyd, R., 2011, Mechanisms controlling the clustering of fluvial channels and the compensational stacking of cluster belts: Journal of Sedimentary Research, v. 81, p. 670–685.

Huling, G., and Holbrook, J., 2016, Clustering of elongate muddy delta lobes within fluviolacustrine systems, Jurassic Kayenta Formation, Utah: Autogenic Dynamics and Self-Organization in Sedimentary Systems: SEPM (Society for Sedimentary Geology) Special Publication, no. 106.

Koch, A.R., 2018, Statistical comparison of fluvial channel belt clustering and architectural metrics, Cretaceous John Henry Member, Straight Cliffs Formation, Utah, United States of America [M.S. thesis]: University of Utah, 177 p.

Jerolmack, D.J., and Paola, C., 2007, Complexity in a cellular model of river avulsion: Geomorphology, v. 91, p. 259–270.

Johnson, C.L., Stright, L., Purcell, R., and Durkin, P., 2016, Stratigraphic evolution of an estuarine fill succession and the reservoir characterization of inclined heterolithic strata , Cretaceous of southern Utah , USA: Geological Society, London, Special Publications, v. 444, p. 251-286.

Larue, D.K., and Hovadik, J., 2006, Connectivity of channelized reservoirs: a modelling approach: Petroleum Geoscience, v. 12, p. 291–308.

Lawton, T.F., Schellenbach, W.L., and Nugent, A.E., 2014, Megafan and axial-river systems in the southern Cordilleran foreland basin: Drip Tank Member of Straight Cliffs Formation and adjacent strata, southern Utah, USA: Journal of Sedimentary Research, v. 84, p. 407–434.

Leeder, M.R., 1978, A quantitative stratigraphic model for alluvium with special reference to channel deposit density and interconnectedness: Fluvial Sedimentology, Memoir 5, p. 587–596

Little, W.W., 1997, Tectonic and eustatic controls on cyclical fluvial patterns, Upper Cretaceous strata of the Kaiparowits Basin, Utah: Learning from the land: Grand Staircase – Escalante National Monument science symposium proceedings: Salt Lake City, p. 489–504.

Liu, S., and Nummedal, D., 2004, Late Cretaceous subsidence in Wyoming: Quantifying the dynamic component. Geology, v. 32, no. 5, p. 397-400.

Liu, S., Nummedal, D., and Liu, L., 2011, Migration of dynamic subsidence across the Late Cretaceous United States Western Interior Basin in response to Farallon plate subduction: Geology, v. 39, p. 555–558.

McHargue, T., Pyrcz, M.J., Sullivan, M.D., Clark, J.D., Fildani, A., Romans, B.W., Covault, J. A., Levy, M., Posamentier, H.W., and Drinkwater, N.J., 2011, Architecture of turbidite channel systems on the continental slope: Patterns and predictions: Marine and Petroleum Geology, v. 28, p. 728–743.

Miall, A.D., 1988, Facies architecture in clastic sedimentary basins, *in* New perspectives in basin analysis, Springer, p. 67–81.

Mohrig, D., Heller, P.L., Paola, C., and Lyons, W.J., 2000, Interpreting avulsion processes from ancient alluvial sequences: Guadalope-Matarranya system (northern Spain) and Watsch Formation (western Colorado): Geological Society of America Bulletin, v. 112, p. 1787–1803.

Mulhern, J.S., and Johnson, C.L., 2017, Time–space variability of paralic strata deposited in a high accommodation, high sediment supply setting: example from the Cretaceous of Utah: Geological Society, London, Special Publications, v. 444, p. 349-392.

Nesbit, P.R., Durkin, P.R., Hugenholtz, C.H., Hubbard, S.M. and Kucharczyk, M., 2018, 3-D stratigraphic mapping using a digital outcrop model derived from UAV images and structure-from-motion photogrammetry: Geosphere, v. 14, no. 6, p. 2469-2486.

Owen, A., Nichols, G.J., Hartley, A.J., Weissmann, G.S., and Scuderi, L.A., 2015, Quantification of A distributive fluvial system: The Salt Wash DFS of the Morrison: Journal of Sedimentary Research, v. 85, p. 544–561.

Painter, C. S., and Carrapa, B., 2013, Flexural versus dynamic processes of subsidence in the North American Cordillera foreland basin. Geophysical Research Letters, v. 40, no. 16, p. 4249-4253.

Paola, C., 2016, A mind of their own: Recent advances in autogenic dynamics in rivers and deltas: SEPM (Society for Sedimentary Geology) Special Publication, no. 106, p. 5–17.

Paola, C., 2000, Quantitative models of sedimentary basin filling: Sedimentology, v. 47, p. 121–178.

Paola, C., and Mohrig, D., 1996, Palaeohydraulics revisited: Palaeoslope estimation in coarse-grained braided rivers: Basin Research, v. 8, p. 243–254.

Peter, C., Sacchi, Q., Serazio, C., and Verga, F., 2017, Capturing channelized reservoir connectivity uncertainty with amalgamation curves: Marine and Petroleum Geology, v. 88, p. 329–342.

Peterson, F., 1969a, Cretaceous sedimentation and tectonism in the southeastern Kaiparowits Region, UT: U.S. Geological Survey, Open-File Report 1314, 259 p.

Peterson, F., 1969b, Four New Members of the Upper Cretaceous Straight Cliffs Formation in the Southeastern Kaiparowits Region Kane County, Utah: Geological Survey Bulletin, p. J1–J28.

Posamentier, H.W., and Vail, P.R., 1988, Eustatic controls on clastic deposition II — Sequence and systems tract models: The Society of Economic Paleontologists and Mineralogists, p. 125–154.

Primm, J.W., Johnson, C.L., and Stearns, M., 2017, Basin-axial progradation of a sediment supply driven distributive fluvial system in the Late Cretaceous southern Utah foreland: Basin Research, v. 30, p. 249–278.

Rittersbacher, A., Howell, J. A., and Buckley, S.J., 2014, Analysis of fluvial architecture in the Blackhawk Formation, Wasatch Plateau, Utah, U.S.A., using large 3D photorealistic models: Journal of Sedimentary Research, v. 84, p. 72–87.

Robinson, J.W., and McCabe, P.J., 1997, Sandstone-body and shale-body dimensions in a braided fluvial system: Salt wash sandstone member (Morrison formation), Garfield County, Utah: AAPG Bulletin, v. 81, p. 1267–1291.

Shanley, K.W., and McCabe, P.J., 1993, Alluvial architecture in a sequence stratigraphic framework: A case history from the Upper Cretaceous of southern Utah, USA: , p. 21–56.

Shanley, K.W., and McCabe, P.J., 1991, Predicting facies architecture through sequence stratigraphy - an example from the Kaiparowits Plateau, Utah: Geology, v. 19, p. 742–745.

Shanley, K.W., and McCabe, P.J., 1995, Sequence stratigraphy of Turonian-Santonian strata, Kaiparowits Plateau, southern Utah, USA: Implications for regional correlation and foreland basin evolution, *in* Van Wagoner, J.C. and Bertram, G.G., eds., Sequence Stratigraphy of Foreland Basin Deposits, Outcrop and Subsurface Examples from the Cretaceous of North America: American Association of Petroleum Geologists, Memoir 64, p. 103-136.

Straub, K.M., Paola, C., Mohrig, D., Wolinsky, M. A., and George, T., 2009, Compensational stacking of channelized sedimentary deposits: Journal of Sedimentary Research, v. 79, p. 673–688.

Szwarc, T.S., Johnson, C.L., Stright, L.E., and McFarlane, C.M., 2015, Interactions between axial and transverse drainage systems in the Late Cretaceous Cordilleran foreland basin : Evidence from detrital zircons in the Straight Cliffs Formation , southern Utah, USA: , p. 372–392.

Weissmann, G.S., Hartley, A.J., Nichols, G.J., Scuderi, L.A., Olson, M., Buehler, H., and Banteah, R., 2010, Fluvial form in modern continental sedimentary basins: Distributive fluvial systems: Geology, v. 38, p. 39–42.

Westoby, M.J., Brasington, J., Glasser, N.F., Hambrey, M.J., and Reynolds, J.M., 2012, "Structure-from-Motion" photogrammetry: A low-cost, effective tool for geoscience applications: Geomorphology, v. 179, p. 300–314.

Wright, V.P., and Marriott, S.B., 1993, The sequence stratigraphy of fluvial depositional systems: The role of floodplain sediment storage: Sedimentary Geology, v. 86, p. 203–210.

FIGURE CAPTIONS

Figure 1 - Modified from Gooley et al. (2016). Map of the Kaiparowits Plateau, highlighting regional outcropping of the John Henry Member (gray), general paleogeography, field locations of the current study (the Cockscomb, CC1 and CC5) and past studies (Rock House Cove and Bull Canyon). Locations of measured sections are indicated by bold points, and areas collected as digital outcrop models are indicated by labeled polygons in the 'Areas of Interest' expansion of the map. Rose diagrams show paleocurrent indicators collected in this (The Cockscomb) and previous studies (Rock House Cove and Bull Canyon, Gooley et al. 2016). Fm = Formation; WIS = Western Interior Seaway.

Figure 2 - Digital outcrop model (DOM) of outcrop CC1 created using stereophotogrammetry. The top image is the uninterpreted DOM, and the bottom image is with channel belt interpretations (white polygons). North is to the left of the image. Interpretations span the entire John Henry Member, bounded by the contacts with the underlying Smoky Hollow Member (red), and the overlying Drip Tank Member (blue). Measured sections CCX.2 (left) and CCX.3 (right) show facies and grain size (M = mud; S = sand, and G = gravel), and are correlated to the DOM image with major formation contacts. Double-sided arrows indicate the distance each measured section is away from the DOM edge. Note that the scale of the DOM and measured sections are different.

Figure 3 – Digital outcrop models of outcrop CC5 created using stereophotogrammetry. The outcrop is covered by a northern (A) and southern (B) DOM. The interpretations from both DOMs were combined for data analysis. The top image of each DOM is uninterpreted, and the

bottom image is with channel belt interpretations (white polygons). North is to the left of the image. Interpretations span the entire John Henry Member, bounded by the contact with the underlying Smoky Hollow Member (red), and the overlying Drip Tank Member (blue). Measured section CCX.1 shows facies and grain size, and is correlated to the DOM image with major formation contacts. Note that the scale of the DOMs and measured section are different.

Figure 4 - Example of the bounding surface hierarchy method employed to interpret the Cockscomb DOMs. Numbers indicate the bounding surface hierarchy level, following the methods of Miall (1988), with question marks for surfaces of uncertain hierarchy. See text for further description of this method. A) Uninterpreted DOM image of a channel belt within outcrop CC5, which has higher resolution than the DOM on average. B) Detailed interpretation of bounding surfaces visible in image A. C) Interpretation that would likely result from this same outcrop at a lower resolution, such as the average resolution for the rest of this DOM.

Figure 5 - Illustrations of how NTG (A), amalgamation (B), and channel belt width and thickness (C) are calculated within a moving window. See methods section for explanation of variables.

Figure 6 – Plots of channel belts (gray polygons) and their centroids (black points) for CC1 (A), and CC5 (B). Red rectangles illustrate the 600 x 25 m moving window used to average architectural metrics (i) and the moving window spanning the entire outcrop width to capture gross vertical trends (ii). C) Channel belt centroid points of outcrop CC5 with blue quadrat cells within a red moving window, illustrating one window at small scale (iii), medium scale (iv), and large scale (v) point pattern analyses. The dimensions of each of these scales are listed Table 1.

Stratigraphic subdivisions of lower, middle, and upper units are denoted with dashed lines. Vertical exaggeration for both outcrops is 2.5x.

Figure 7 – Modified from Figure 5 from Benhallam et al. (2016). A) Examples of uniform, random, and clustered point patterns. B) Demonstration of the quadrat method performed on the entire window, and the resulting relationship of variance to mean for each type of point pattern.

Figure 8 – A-H: Outcrop properties averaged over moving windows 600 m wide by 25 m thick, moving vertically by 5 m increments, and laterally by 50 m increments, for outcrops CC1 (left) and CC5 (right). I-P: Outcrop properties averaged over moving windows spanning the entire outcrop width and 25 m thick, moving vertically by 5 m increments, for outcrops CC1 (left) and CC5 (right). All properties are shaded from white (low) to black (high) with a linear gradient. The minimum and maximum values for each plot are indicated inside a white and black box respectively, and encompass the entire range for both outcrops to allow direct comparison. Horizontal dashed lines indicate lower, middle, and upper stratigraphic units, and vertical dashed lines indicate lateral segments.

Figure 9 –Trends of NTG, amalgamation, channel belt width and thickness, and point patterns averaged laterally by outcrop segments; northern (N), central (C), and southern (S). Vertical moving windows 25 m thick, moving in 5 m increments, were used for NTG, amalgamation, and channel belt width and thickness. Point patterns were assigned qualitatively based on the dominant moving window trends in Figure 11. Architectural properties increase from white to black, while point patterns are represented as either gray (uniform), white (random), or black

(clustered). Lower, middle, and upper stratigraphic units are noted by dashed lines and define the vertical scale.

Figure 10 - Histograms and vital statistics of channel belt (CB) widths (top) and thicknesses (bottom) for CC1 (left) and CC5 (right). Arrows on plot ‘CC5 CB Width’ (upper right) are pointing to columns with only one channel belt, for improved visibility. Widths and thicknesses presented are the maximum width and thickness of each individual channel belt. For CC1 n = 104, and for CC5 n = 265.

Figure 11 - Results of the quadrat analysis for both CC5 (A-C) and CC1 (D) at different point pattern scales and aspect ratios. A) CC5 small scale point patterns using quadrat cells 241.5 m wide by 15 m thick, with an aspect ratio of 16:1, and 1800 m wide by 30 m thick moving windows. B) CC5 large scale point patterns using quadrat cells 805 m wide by 50 m thick, with an aspect ratio of 16:1, and 1610 m wide by 100 m thick moving windows. C) CC5 medium scale point patterns using quadrat cells 120 m wide by 50 m thick, with an aspect ratio of 2.4:1, and 960 m wide by 100 m thick moving windows. C) CC1 medium scale point patterns using quadrat cells 120 m wide by 50 m thick, with an aspect ratio of 2.4:1, and 480 m wide by 100 m thick moving windows. E-H) Results of correlation between the corresponding cluster analysis (A-D), and 2D NTG results using the same moving window size.

Figure 12 – Correlations of 1D-to-2D architectural metrics: NTG (left, A and B), amalgamation (middle, C and D), and thickness (right, E and F), for both CC1 (top, A, C, and E) and CC5 (bottom, B, D, and F). The X-axis represents the lateral moving window position increasing from

north to south, and the Y-axis is the correlation coefficient between the 1D and 2D trends for each metric. The inset box within each plot shows the mean, standard deviation, minimum, and maximum R^2 value for its respective analysis.

		Moving Window		Quadrat Cells				
Outcrop	Quadrat Scale	Width (m)	Thickness (m)	Width (m)	Thickness (m)	Number Cells	Aspect Ratio	Figure Reference
CC5	Small	1800	30	241.5	15	16	16.1:1	Fig. 6iii
	Medium	960	100	120	50	16	2.4:1	Fig. 6iv
	Large	1610	100	805	50	4	16.1:1	Fig. 6v
CC1	Medium	480	100	120	50	8	2.4:1	Half the width of grid in Fig. 6iv

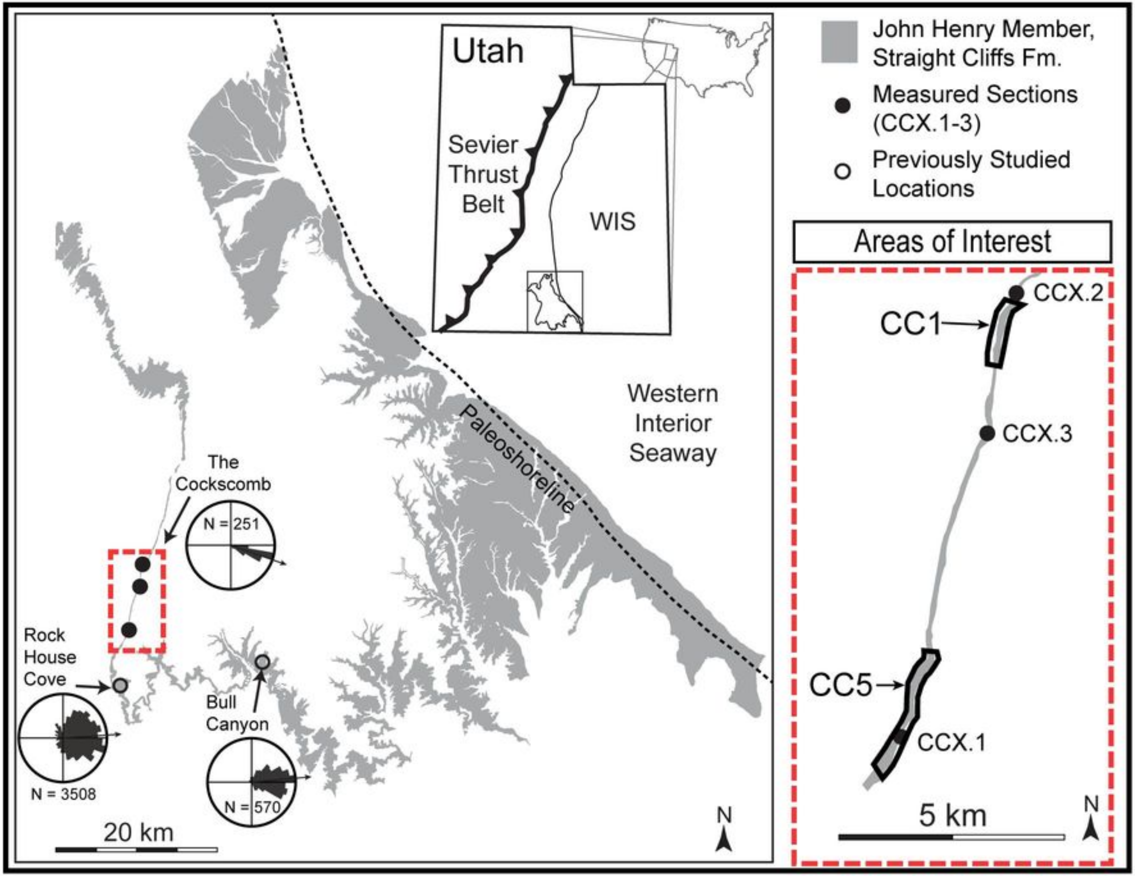
Utah
Sevier
Thrust
Belt
WIS
Western
Interior
Seaway
Paleoshoreline
The
Cockscomb
N = 251
Rock
House
Cove
N = 3508
Bull
Canyon
N = 570
20 km
N
John Henry Member,
Straight Cliffs Fm.
Measured Sections
(CCX.1-3)
Previously Studied
Locations
Areas of Interest
CCX.2
CC1
CCX.3
CC5
CCX.1
5 km
N

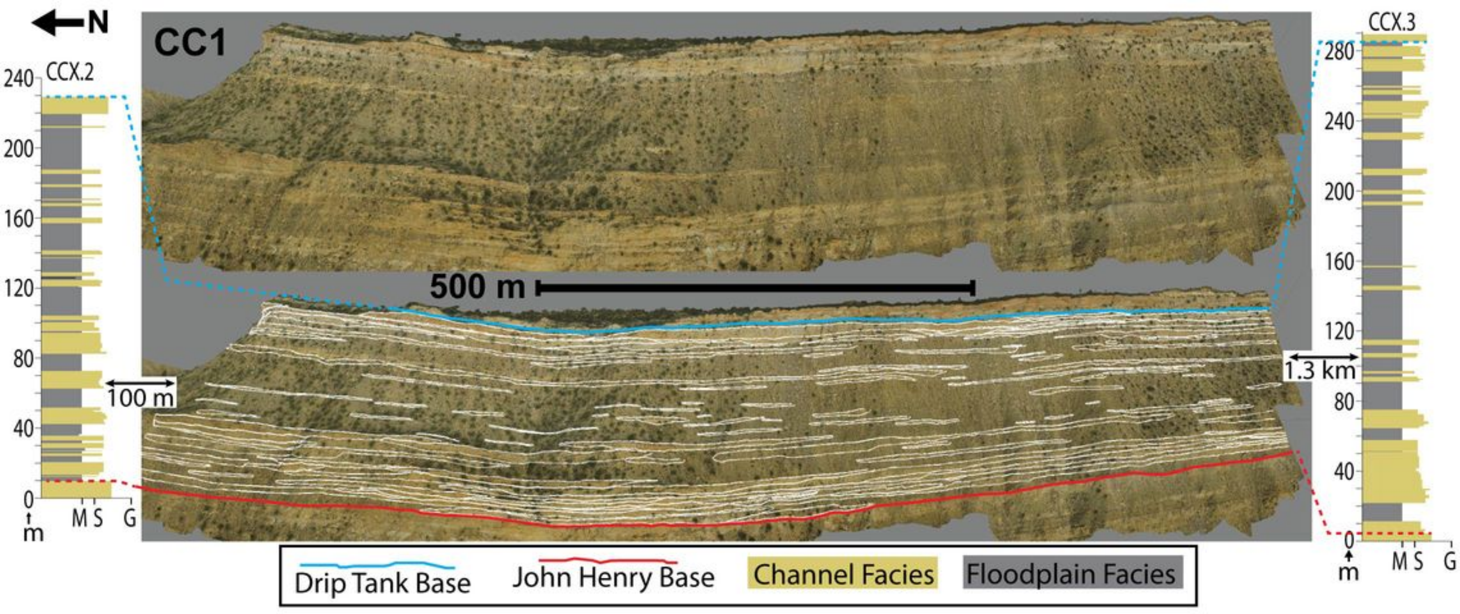
N
CC1
CCX.2
CCX.3
500 m
100 m
1.3 km
240
200
160
120
80
40
0
m
M S G
280
Drip Tank Base
John Henry Base
Channel Facies
Floodplain Facies

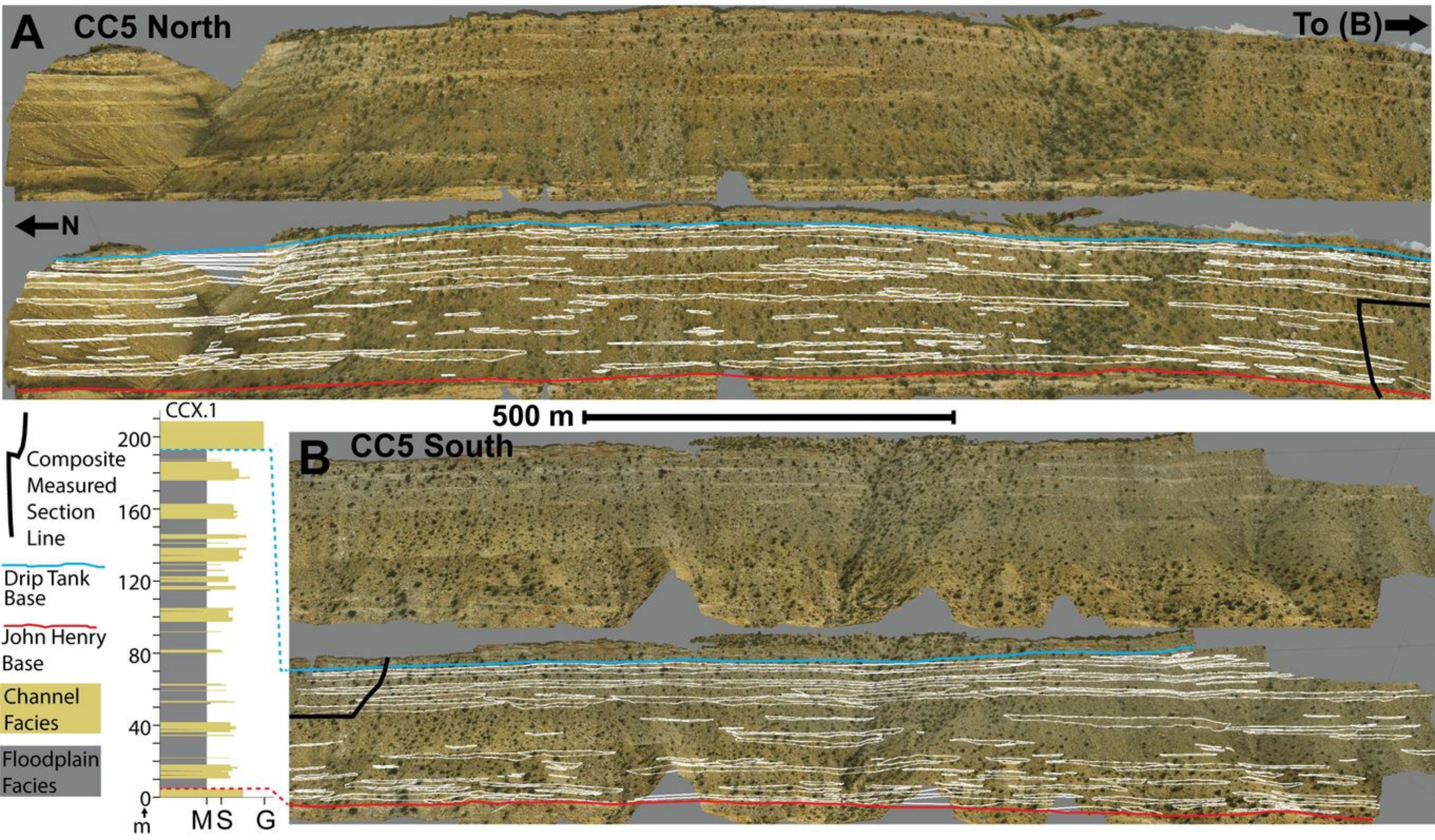

A
CC5 North
To (B)
N
500 m
CCX.1
200
160
120
80
40
0
m
M
S
G
Composite
Measured
Section
Line
Drip Tank
Base
John Henry
Base
Channel
Facies
Floodplain
Facies
B
CC5 South

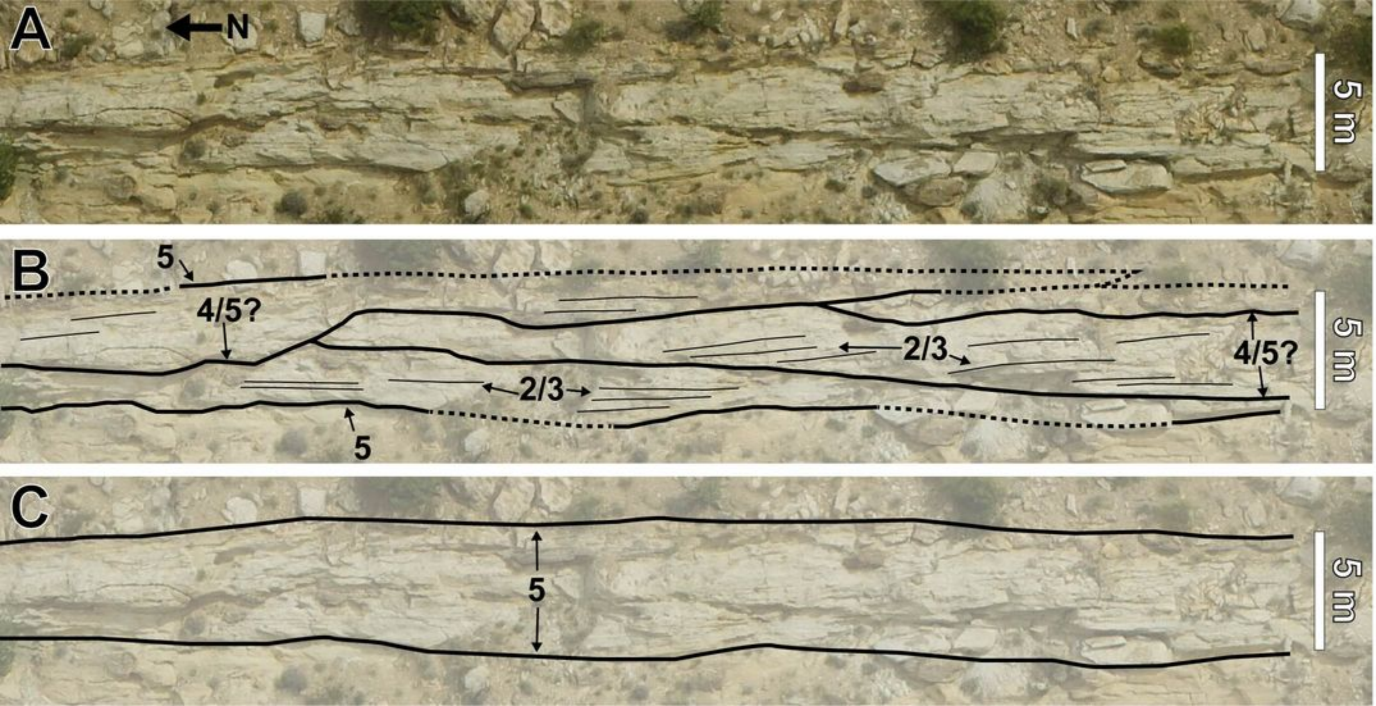
A
N
5 m
B
5
4/5?
2/3
2/3
4/5?
5
5 m
C
5
5 m

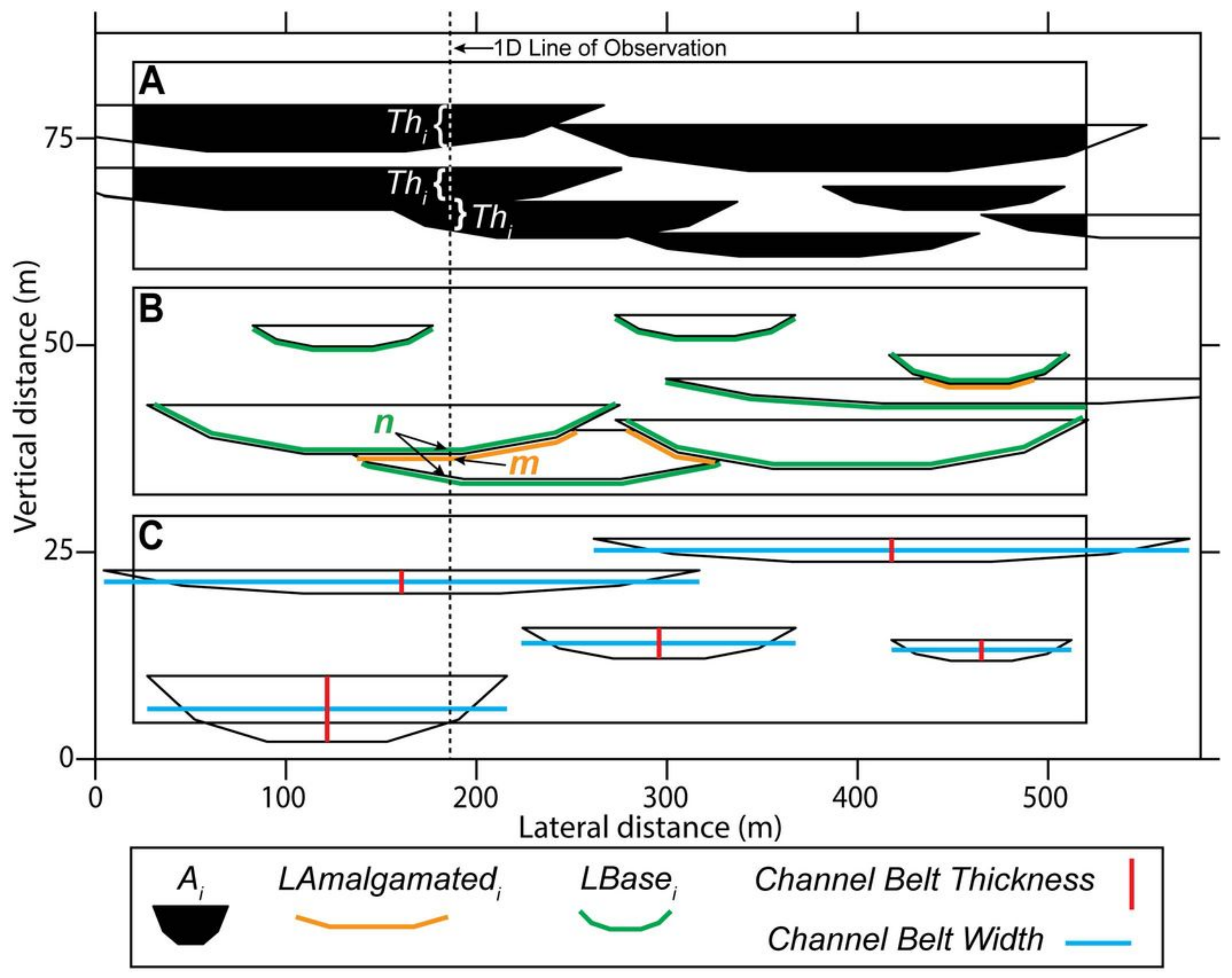
1D Line of Observation
A
B
C
Th_i
n
m
Vertical distance (m)
Lateral distance (m)
0
25
50
75
100
200
300
400
500
A_i
LAmalgamated_i
LBase_i
Channel Belt Thickness
Channel Belt Width

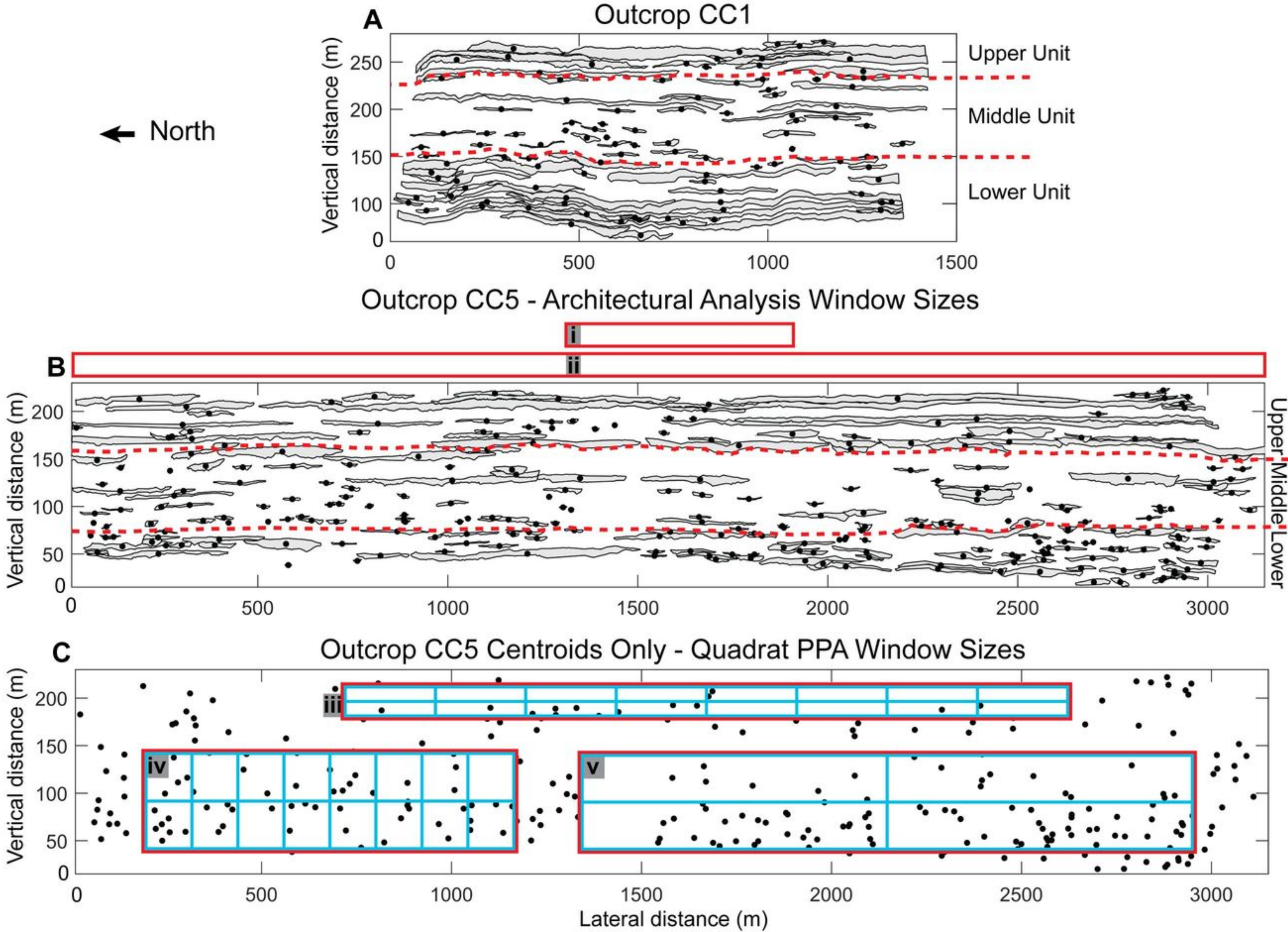
A
Outcrop CC1
Upper Unit
Middle Unit
Lower Unit
North
Vertical distance (m)
Outcrop CC5 - Architectural Analysis Window Sizes
i
ii
B
Upper
Middle
Lower
C
Outcrop CC5 Centroids Only - Quadrat PPA Window Sizes
iii
iv
v
Lateral distance (m)

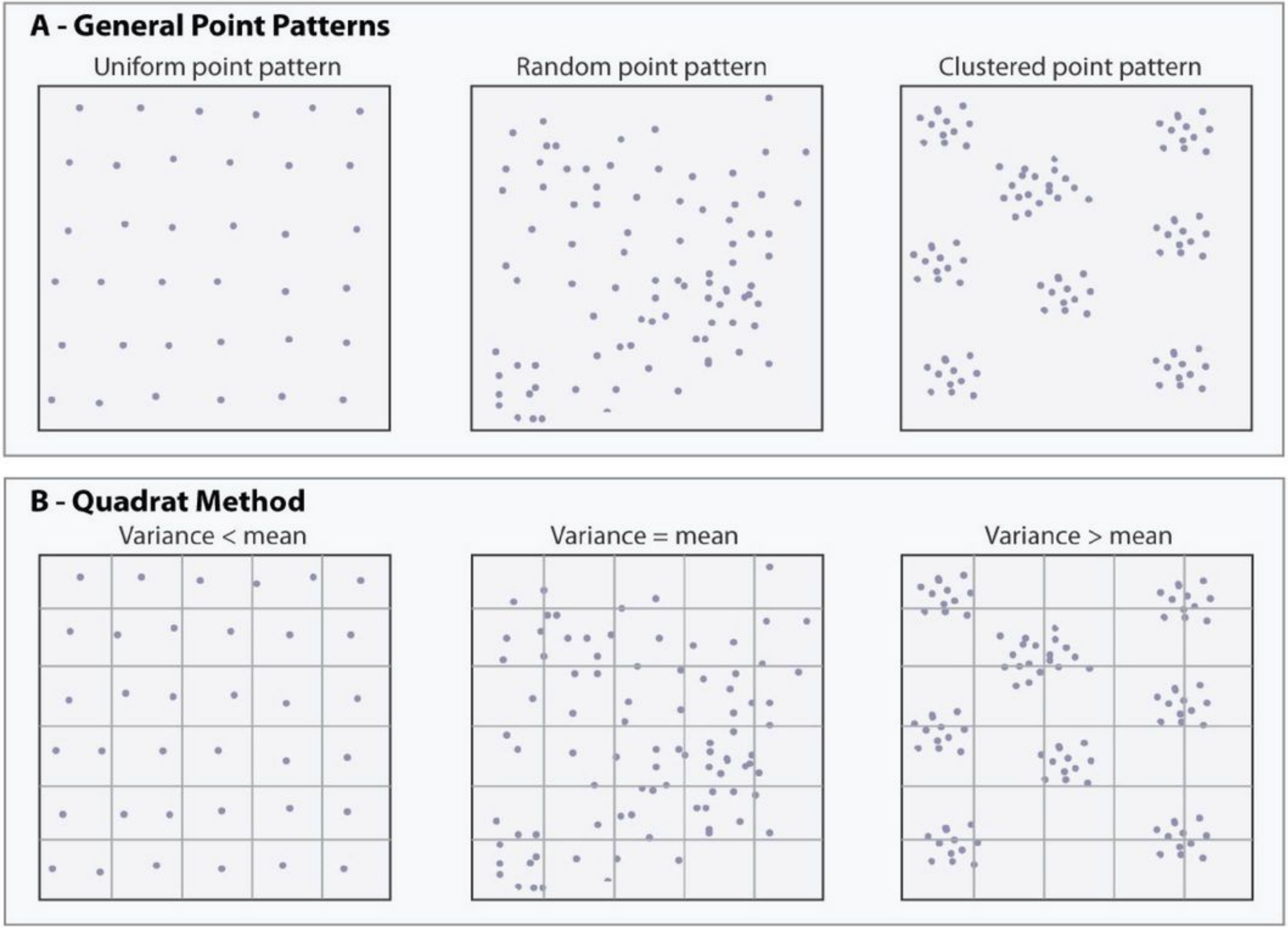

A - General Point Patterns
Uniform point pattern
Random point pattern
Clustered point pattern
B - Quadrat Method
Variance < mean
Variance = mean
Variance > mean

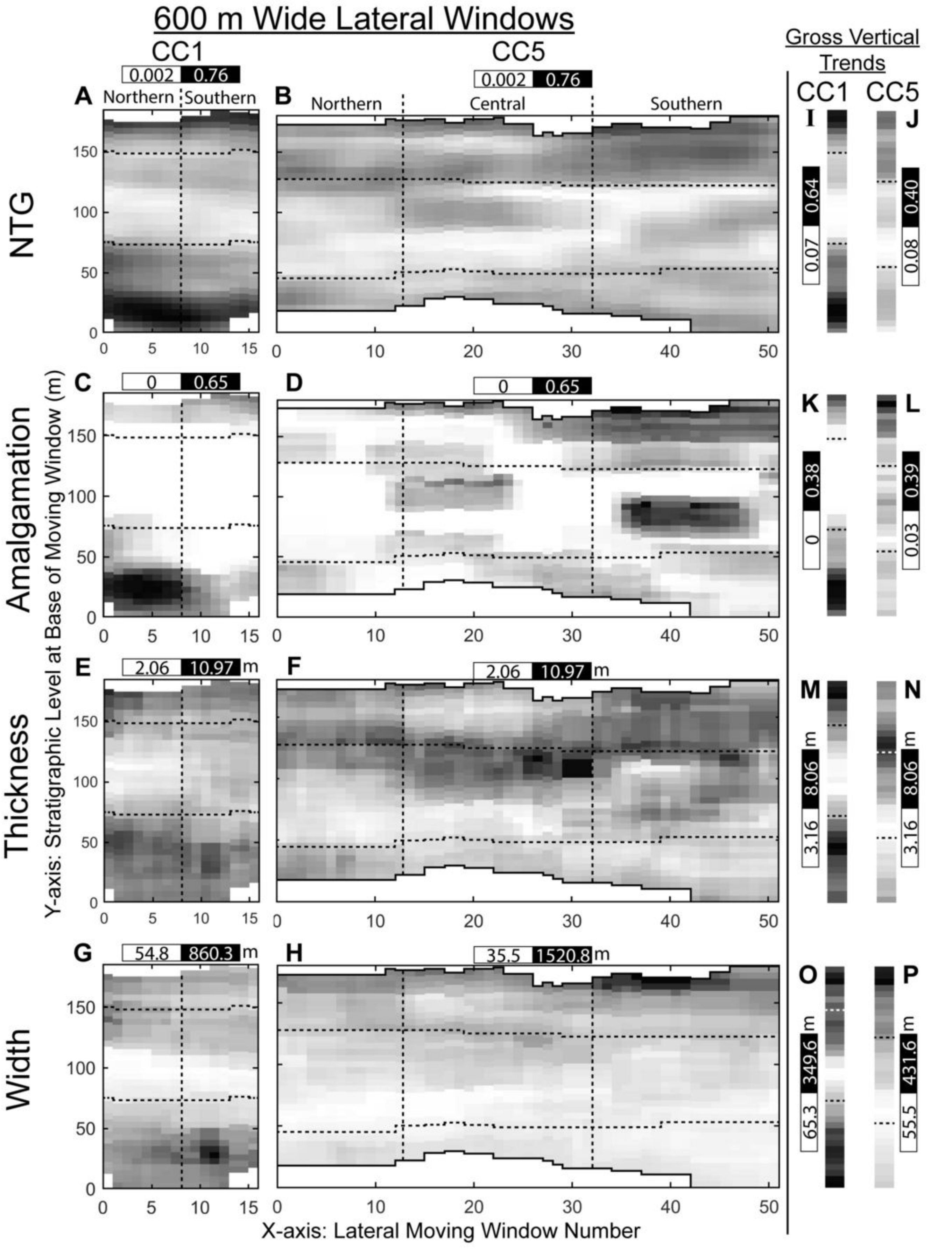
600 m Wide Lateral Windows
CC1
CC5
Gross Vertical Trends
NTG
Amalgamation
Thickness
Width
Northern
Southern
Central
0.002
0.76
0
0.65
2.06
10.97 m
54.8
860.3 m
35.5
1520.8 m
0.64
0.07
0.40
0.08
0.38
0
0.39
0.03
8.06
3.16
349.6
65.3
431.6
55.5
Y-axis: Stratigraphic Level at Base of Moving Window (m)
X-axis: Lateral Moving Window Number

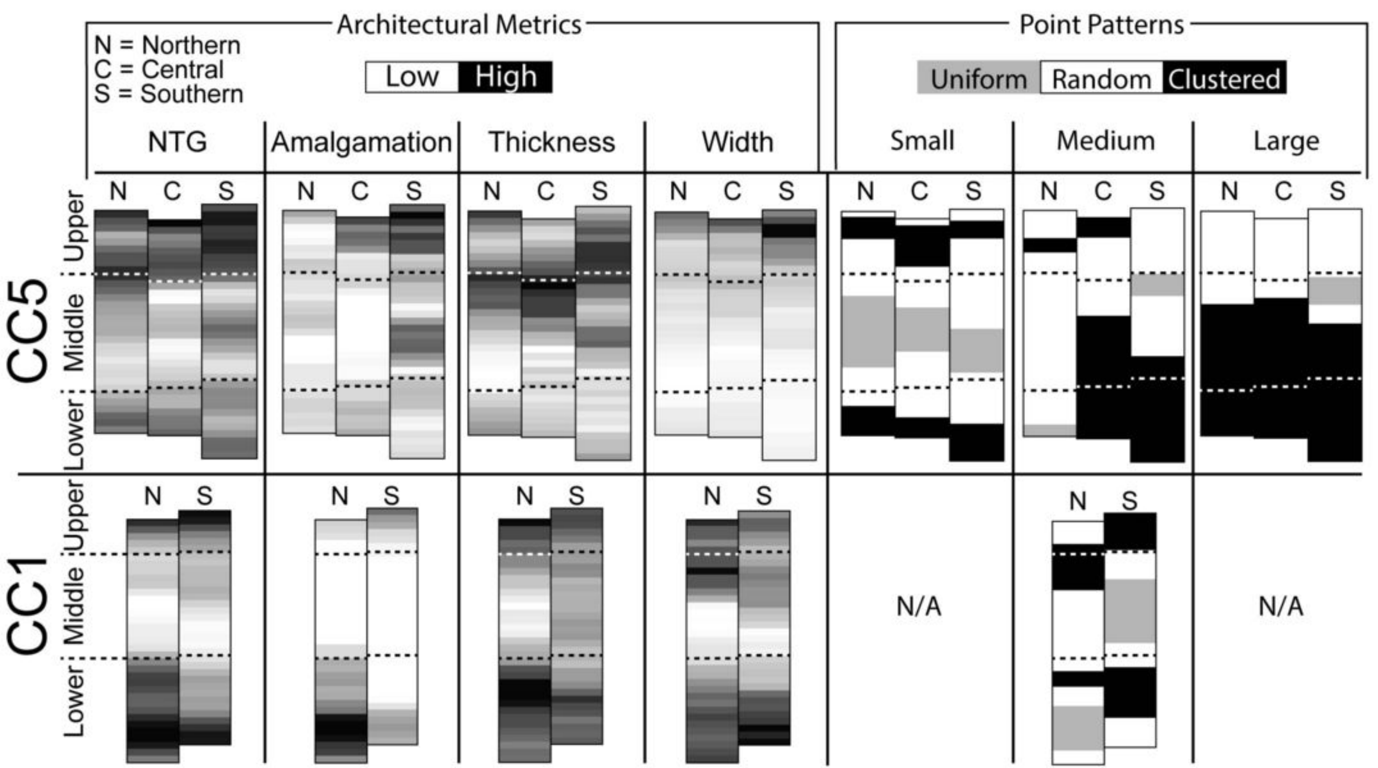

Architectural Metrics
N = Northern
C = Central
S = Southern
Low
High
Point Patterns
Uniform
Random
Clustered
NTG
Amalgamation
Thickness
Width
Small
Medium
Large
N C S
CC5
Upper
Middle
Lower
CC1
N S
N/A
N/A

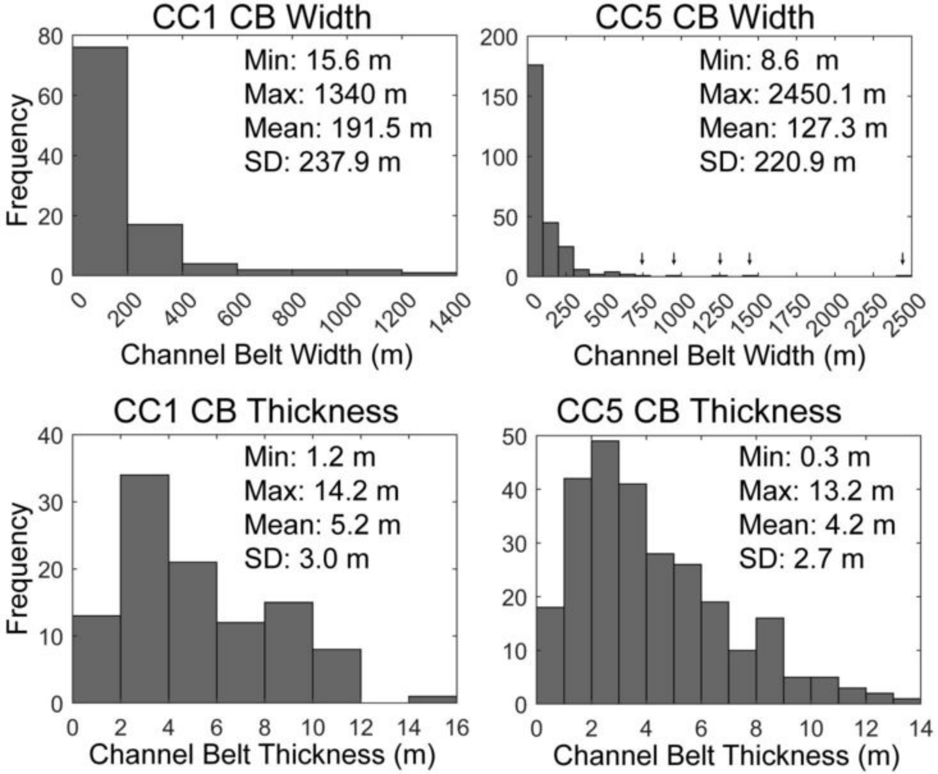
CC1 CB Width
Min: 15.6 m
Max: 1340 m
Mean: 191.5 m
SD: 237.9 m
Frequency
Channel Belt Width (m)
CC5 CB Width
Min: 8.6 m
Max: 2450.1 m
Mean: 127.3 m
SD: 220.9 m
Channel Belt Width (m)
CC1 CB Thickness
Min: 1.2 m
Max: 14.2 m
Mean: 5.2 m
SD: 3.0 m
Frequency
Channel Belt Thickness (m)
CC5 CB Thickness
Min: 0.3 m
Max: 13.2 m
Mean: 4.2 m
SD: 2.7 m
Channel Belt Thickness (m)

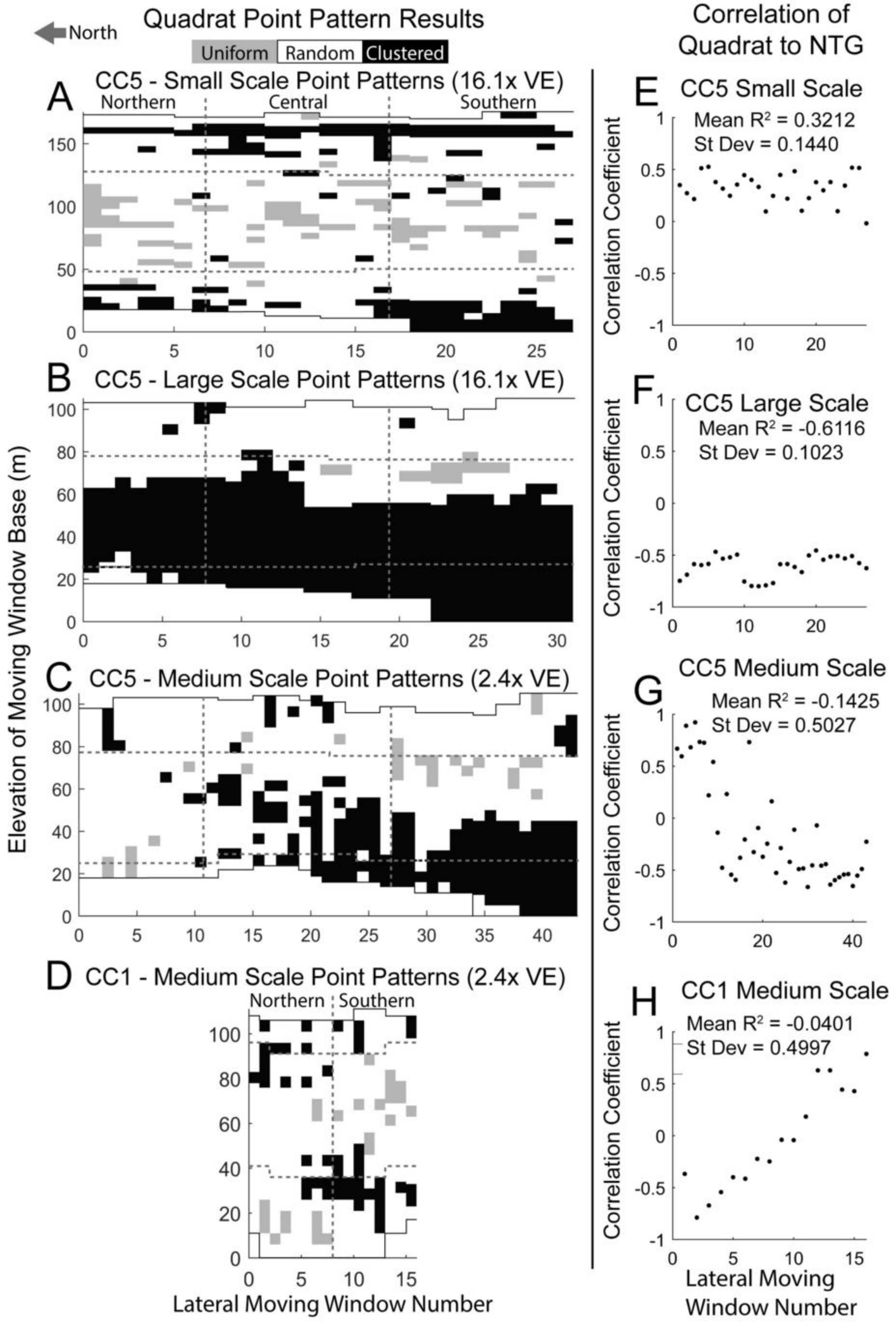
North
Quadrat Point Pattern Results
Uniform
Random
Clustered
Correlation of Quadrat to NTG
A
CC5 - Small Scale Point Patterns (16.1x VE)
Northern
Central
Southern
B
CC5 - Large Scale Point Patterns (16.1x VE)
C
CC5 - Medium Scale Point Patterns (2.4x VE)
D
CC1 - Medium Scale Point Patterns (2.4x VE)
Northern
Southern
Elevation of Moving Window Base (m)
Lateral Moving Window Number
E
CC5 Small Scale
Mean R² = 0.3212
St Dev = 0.1440
F
CC5 Large Scale
Mean R² = -0.6116
St Dev = 0.1023
G
CC5 Medium Scale
Mean R² = -0.1425
St Dev = 0.5027
H
CC1 Medium Scale
Mean R² = -0.0401
St Dev = 0.4997
Correlation Coefficient
Lateral Moving Window Number

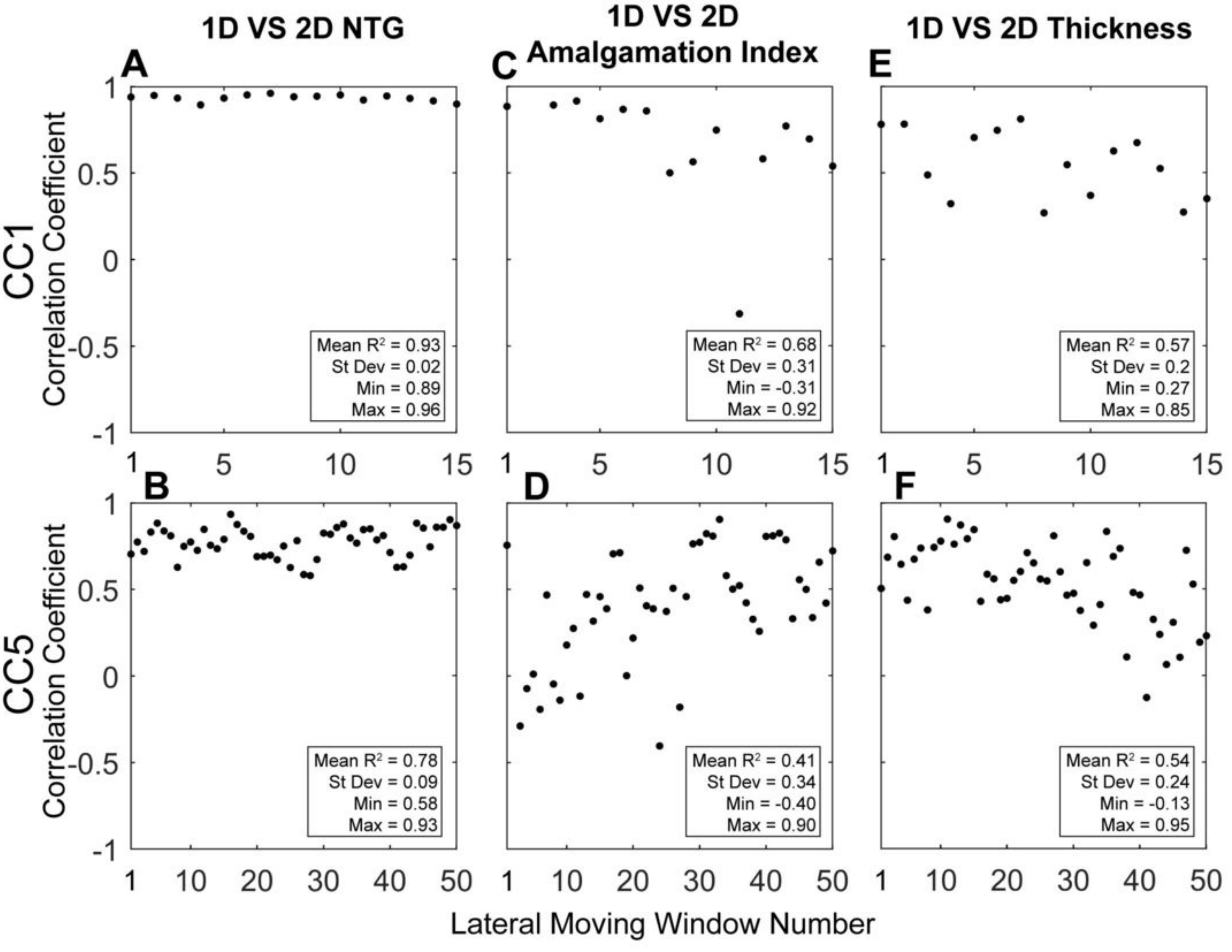
1D VS 2D NTG
1D VS 2D
Amalgamation Index
1D VS 2D Thickness
A
C
E
B
D
F
CC1
CC5
Correlation Coefficient
Mean R² = 0.93
St Dev = 0.02
Min = 0.89
Max = 0.96
Mean R² = 0.68
St Dev = 0.31
Min = -0.31
Max = 0.92
Mean R² = 0.57
St Dev = 0.2
Min = 0.27
Max = 0.85
Mean R² = 0.78
St Dev = 0.09
Min = 0.58
Max = 0.93
Mean R² = 0.41
St Dev = 0.34
Min = -0.40
Max = 0.90
Mean R² = 0.54
St Dev = 0.24
Min = -0.13
Max = 0.95
Lateral Moving Window Number